Neural Basis for Regulation of Vasopressin Secretion by Anticipated Disturbances in Osmolality

Angela Kim[1, 2], Joseph C. Madara[1], Chen Wu[1], Mark L. Andermann[1, 2], Bradford B. Lowell[1, 2]

[1] Division of Endocrinology, Diabetes, and Metabolism, Department of Medicine, Beth Israel Deaconess Medical Center, Harvard Medical School, Boston, MA 02215, USA

[2] Program in Neuroscience, Harvard Medical School, Boston, MA 02215, USA

Correspondence should be addressed to: Bradford B. Lowell (blowell@bidmc.harvard.edu)

Abstract

Water balance, tracked by extracellular osmolality, is regulated by feedback and feedforward mechanisms. Feedback regulation is reactive, occurring as deviations in osmolality are *detected*. Feedforward or presystemic regulation is proactive, occurring when disturbances in osmolality are *anticipated*. Vasopressin (AVP) is a key hormone regulating water balance and is released during hyperosmolality to limit renal water excretion. AVP neurons are under feedback and feedforward regulation. Not only do they respond to disturbances in blood osmolality, but they are also rapidly suppressed and stimulated, respectively, by drinking and eating, which will ultimately decrease and increase osmolality. Here, we demonstrate that AVP neuron activity is regulated by multiple anatomically- and functionally-distinct neural circuits. Notably, presystemic regulation during drinking and eating are mediated by non-overlapping circuits that involve the lamina terminalis and hypothalamic arcuate nucleus, respectively. These findings reveal neural mechanisms that support differential regulation of AVP release by diverse behavioral and physiological stimuli.

Introduction

Rapid, anticipatory feedforward regulation is a common feature of many homeostatic circuits (Betley et al., 2015; Zimmerman et al., 2016; Augustine et al., 2018). While the purpose of feedforward regulation has yet to be established, a number of compelling proposals have been suggested. Several studies have shown that feedforward regulation plays an important role in shaping ingestive behavior by promoting negative-reinforcement learning (Betley et al., 2015; Allen et al., 2017; Leib et al., 2017). It is also suggested that feedforward regulation is crucial for maintaining energy/water balance as it prevents overconsumption by preemptively terminating ingestive behavior before systemic disturbance is detected (Andermann and Lowell, 2017; Augustine et al., 2020). Although the significance of feedforward regulation is just beginning to be recognized, the idea of such regulation in the hypothalamus existed since the late 1900s. A conceptual framework for feedforward regulation was provided by studies looking at the effect of water intake on blood vasopressin (AVP) levels, from which the term ‘presystemic regulation’ originates (Stricker and Hoffmann, 2007).

AVP, also known as antidiuretic hormone, is synthesized by posterior pituitary-projecting magnocellular AVP neurons of the paraventricular (PVH) and supraoptic nuclei (SON) of the hypothalamus. These neurons underlie the body’s main non-behavioral response to dehydration or elevated systemic osmolality - an increase in circulating AVP. Upon stimulation of AVP neurons, AVP is released from the axon terminals in the posterior pituitary and enters the bloodstream (Ferguson et al., 2003; Bolignano et al., 2014). Once released, AVP binds to receptors in the kidney and

stimulates water reabsorption to restore water balance (Nielsen et al., 1995). Activity of AVP neurons is regulated by two temporally distinct mechanisms. Feedback or systemic regulation, which mainly informs AVP neurons of changes in systemic water balance, is mediated by the lamina terminalis (LT), comprised of the subfornical organ (SFO), median preoptic nucleus (MnPO), and organum vasculosum lamina terminalis (OVLT) (McKinley et al., 2004). The SFO and OVLT are circumventricular organs (CVOs) that lack a blood-brain barrier, and are capable of sensing systemic osmolality and blood-borne factors, such as angiotensin II. Osmolality information sensed by the SFO and OVLT is then sent to AVP neurons directly or indirectly via the MnPO. Feedforward or presystemic regulation, on the other hand, informs AVP neurons of anticipated future osmotic perturbation, based on the array of presystemic signals that occur immediately before (pre-ingestive) and after (post-ingestive) food or water ingestion (Stricker and Hoffmann, 2007; Stricker and Stricker, 2011).

Presystemic regulation of AVP release was first described in 1980, in a study using dehydrated dogs (Thrasher et al., 1981; Thrasher et al., 1987), and was later replicated in humans, monkeys, sheep, and rats (Arnauld and du Pont, 1982; Geelen et al., 1984; Blair-West et al., 1985; Huang et al., 2000). These studies demonstrated that drinking causes a rapid reduction in blood AVP levels and that this decrease precedes any detectable decrease in blood osmolality (i.e. it is presystemic). However, due to lack of temporal resolution in blood AVP measurements (Christ-Crain and Fenske, 2016), these studies failed to capture rapid dynamics of presystemic regulation, preventing further dissection of distinct stimuli causing the presystemic reductions in AVP.

In a previous study, we demonstrated that magnocellular AVP neurons are under bidirectional presystemic regulation by drinking and eating (Mandelblat-Cerf et al., 2017). However, the neural inputs providing presystemic information to these neurons are still unclear. Here, we used various circuit mapping techniques, *in vivo* calcium imaging and opto- and chemo-genetics to identify and characterize the neural circuits mediating presystemic regulation of AVP neuron activity.

Results

AVP neurons receive inhibitory and excitatory inputs from the LT

As the presystemic regulation of AVP neurons is rapid, it must be brought about by neural afferent inputs. To identify these afferents, we performed retrograde rabies mapping from posterior pituitary -projecting, magnocellular SON^{AVP} and PVH^{AVP} neurons using *AVP-IRES-Cre* mice (Figure 1a,e). Cre-dependent TVA (EnvA receptor) (AAV-DIO-TVA) and rabies glycoprotein (RG) (AAV-DIO-RG) viruses were injected into the SON or PVH. Three weeks later, EnvA-pseudotyped G-deleted rabies virus (RV-EnvA-ΔG-GFP) was injected into the SON or posterior pituitary as described below. In order to target magnocellular SON^{AVP} neurons, we injected rabies virus directly into the SON (Figure1a). Note that all AVP neurons in the SON project to the posterior pituitary (Brown et al., 2013; Mandelblat-Cerf et al., 2017). In contrast, the PVH contains magnocellular and non-posterior pituitary-projecting, parvocellular AVP neurons. In order to specifically target magnocellular neurons, we devised a retrograde approach in which rabies virus was injected into the posterior pituitary instead of the PVH (Figure1e).

Because TVA, in addition to being expressed at the cell body, is trafficked to the axon terminals (Betley et al., 2013; Livneh et al., 2017), rabies virus can be taken up by TVA-expressing axons of PVH^{AVP} neurons in the posterior pituitary, leading to projection-specific infection. Starter neurons in the PVH and SON were identified by co-expression of rabies-GFP and TVA-mCherry (Figure1b,f). Remarkably, despite their distinctly different anatomical locations, but in agreement with their identical functions, rabies mapping results from magnocellular PVH^{AVP} and SON^{AVP} neurons were strikingly similar. Both received strong inputs from the SFO, MnPO, and OVLT (Figure 1d,h), and additional sparse rabies labeling was found in the arcuate nucleus (ARC) of the hypothalamus and the perinuclear zone (PNZ), an area surrounding the SON. We also found surprisingly dense rabies labeling in the PVH and SON when inputs to SON^{AVP} and PVH^{AVP} neurons were examined, respectively (Figure 1c,g). We performed additional experiments to investigate these unexpected findings. First, we injected AAV that cre-independently expresses ChR2-mCherry into either the PVH or SON and found that neurons in these sites do not send direct projections to the SON and PVH, respectively. Furthermore, we also injected retrograde tracer cholera toxin subunit B into either the PVH or SON, and in agreement with the above-mentioned anterograde tracing study, failed to detect any labeled neurons in the SON and PVH, respectively (not shown). Based on these results, we believe that axosomatic and axodendritic PVH $\rightarrow$ SON^{AVP} or SON $\rightarrow$ PVH^{AVP} connections do not exist, and we speculate that the above-mentioned rabies results were caused by either non-synaptic transfer of rabies (i.e. an artifact) or synaptic transfer via axoaxonic synapses that might exist between

PVH and SON neurons at the level of the posterior pituitary (Silverman et al., 1983; Choudhury and Ray, 1990).

In order to identify the glutamatergic and GABAergic nature of LT neurons providing inputs to PVH^{AVP} and SON^{AVP} neurons, we performed anterograde tracing from *Vglut2*- versus *Vgat*-expressing neurons of the LT. We injected the cre-dependent synaptophysin (Syn) anterograde tracer, AAV-DIO-Syn-YFP, into the SFO and MnPO/OVLT of *Vglut2-IRES-Cre* and *Vgat-IRES-Cre* mice to individually trace glutamatergic and GABAergic projections (Figure 1i). The MnPO and OVLT were considered as one group because viral targeting of individual structures was challenging. We found that the MnPO/OVLT sends both excitatory and inhibitory projections to the PVH and SON while the SFO only sends excitatory projections (Figure 1j). Lack of long-range inhibitory projections of the SFO has been previously reported (Oka et al., 2015a).

Next, we performed Channelrhodopsin (ChR2)-assisted circuit mapping (CRACM) to test synaptic connectivity of these projections to PVH^{AVP} and SON^{AVP} neurons. AAV-DIO-ChR2-mCherry was injected into the SFO or MnPO/OVLT of *AVP-GFP;Vglut2-IRES-Cre* or *AVP-GFP;Vgat-IRES-Cre* mice and light-evoked postsynaptic currents were recorded from PVH^{AVP} and SON^{AVP} neurons identified by GFP expression (Figure 1k). All SON^{AVP} neurons recorded are magnocellular. We did not distinguish parvocellular and magnocellular PVH^{AVP} neurons in this experiment. We found that SFO^{Vglut2} and $MnPO/OVLT^{Vglut2}$ neurons provided robust glutamatergic input to PVH^{AVP} and SON^{AVP} neurons (Figure 1l,n). In contrast, GABAergic input from $MnPO/OVLT^{Vgat}$ neurons was detected only in half of the PVH^{AVP} and SON^{AVP} neurons. Next, we tested

the synaptic connectivity of the LT to GFP-negative neurons in the PVH and SON (Figure 1m). The MnPO/OVLT provided glutamatergic and GABAergic input to the majority of GFP-negative neurons in the PVH and SON. We did not find any connection between SFO ^{Vglut2} neurons and GFP-negative PVH neurons, suggesting that SFO ^{Vglut2} inputs were highly specific to AVP neurons. Together, these results demonstrate that PVH^{AVP} and SON^{AVP} neurons receive excitatory and inhibitory inputs from the LT.

Water-related presystemic regulation of AVP neurons is mediated by the LT

Next, we examined the involvement of the LT in presystemic regulation of SON^{AVP} neurons. We focused on SON^{AVP} neurons because the magnocellular population can be specifically and efficiently targeted by direct viral injection into the SON. We measured the *in vivo* calcium dynamics of GCaMP6s-expressing SON^{AVP} neurons while inhibiting the MnPO/OVLT or SFO with CNO/hM4Di (Figure 2a,i). To monitor water-related presystemic responses, mice were chronically water-restricted and fully habituated to an experimental paradigm prior to the experiment. At various latencies following the beginning of each session, a water bowl was placed in the cage and mice were allowed to drink freely for ~15 min. Each mouse had one experimental session per day, in which they were pre-injected with either saline or CNO. In the control group, as previously reported (Mandelblat-Cerf et al., 2017), SON^{AVP} neurons were rapidly inhibited as the water bowl was introduced (Figure 2b). This pre-ingestive response was learning-dependent as it gradually developed over the course of training (Figure 2—figure supplement 1). Pre- and post-ingestive suppression of SON^{AVP}

157 neurons were observed before the significant drop in systemic osmolality, which we
158 previously found to begin 10-15 min after drinking onset (Mandelblat-Cerf et al., 2017).
159 Inhibition of the MnPO/OVLT abolished the pre-ingestive drop in SON^{AVP} neuron activity
160 (Figure 2b-f). The post-ingestive response was also significantly attenuated. When
161 recordings were performed from mice expressing the calcium-independent fluorescent
162 marker, EYFP, in SON^{AVP} neurons, no feeding/drinking-induced response was observed
163 (Figure 2—figure supplement 2), demonstrating that the changes in GCaMP6s
164 fluorescence were not due to movement artifacts.

165 Because the MnPO contains thirst-regulating neurons (Abbott et al., 2016;
166 Augustine et al., 2018), we also analyzed drinking behavior in these mice. MnPO/OVLT
167 inhibition did not prevent drinking but delayed drinking onset as demonstrated by a
168 significant increase in the latency to drink (Figure 2g). The number of drinking bouts per
169 session was not affected. The MnPO/OVLT, along with the SFO, are the main sources
170 of excitatory input that underlie activation of SON^{AVP} neurons during systemic
171 hyperosmolality (McKinley et al., 2004). Consistent with this, we found that MnPO/OVLT
172 inhibition caused a drop in the baseline activity of SON^{AVP} neurons in water-restricted
173 mice (Figure 2h). In a separate group of mice, we investigated the effect of SFO
174 inhibition (Figure 2i). Inhibition of the SFO caused a slight but non-significant
175 attenuation of pre- and post-ingestive suppression (Figure 2j-l). Together, these data
176 indicate that neurons in the MnPO/OVLT are important mediators of water-related
177 presystemic signals to AVP neurons.

178

Presystemic signals enter the LT at the level of MnPO

Next, we sought to understand the organization of the presystemic circuit mediating water-related information within and upstream of the LT. Both the SFO and MnPO/OVLT provide strong excitatory inputs to AVP neurons. However, we found that only the MnPO/OVLT was required for water-related presystemic regulation of SON^{AVP} neurons (Figure 2), suggesting that the presystemic circuit might be organized similarly to the hierarchical thirst circuit described previously (Augustine et al., 2018). To test this idea, we mapped inputs to SON-projecting $MnPO/OVLT^{Vglut2}$ and SFO^{Vglut2} neurons using monosynaptic rabies tracing. SON-projecting neurons were targeted using a retrograde approach shown schematically in Figure 3a,d. SON-projecting starter neurons, visualized by coexpression of GFP and mCherry, were seen in the MnPO/OVLT and SFO (Figure 3b,e). Results from the MnPO/OVLT and SFO were strikingly different. SON-projecting $MnPO/OVLT^{Vglut2}$ neurons received inputs from multiple sites (Figure 3c), including the SFO, PVH, ventromedial (VMH), and dorsomedial nuclei (DMH) of the hypothalamus, and the lateral parabrachial nucleus (LPBN). Among these areas, the SFO contained the greatest number of rabies-labeled neurons, demonstrating strong interconnectivity between these LT structures. In contrast, SON-projecting SFO^{Vglut2} neurons received inputs only from the other LT structures, the MnPO and OVLT (Figure 3f). The result was further validated using *Nos-1-IRES-Cre* mice, another cre line that specifically marks excitatory SFO neurons (Figure 3—figure supplement 1) (Zimmerman et al., 2016). These data demonstrate that the MnPO/OVLT is the only LT region that directly receives and relays extra-LT

inputs to AVP neurons and, thus, is likely the main entry point for water-related presystemic information to the LT.

Collateralization of SON-projecting LT neurons

Magnocellular PVH^{AVP} and SON^{AVP} neurons, despite their distinct anatomical locations, are functionally identical, receive inputs from the same sites (Figure 1), and show similar presystemic responses (Mandelblat-Cerf et al., 2017). To explore the possibility that presystemic regulation of both PVH^{AVP} and SON^{AVP} neurons is mediated by collateral projections from the same LT neurons, we performed rabies-based axon collateral mapping from SON-projecting MnPO/OVLT^{Vglut2}, MnPO/OVLT^{Vgat}, and SFO^{Vglut2} neurons and examined their collateral projections in the LT, PVH, and SON. Rabies-based axon collateral mapping was performed as previously described (Betley et al., 2013; Livneh et al., 2017; Livneh et al., 2020). We found rabies-labeled collateral projections of SON-projecting MnPO/OVLT^{Vglut2}, MnPO/OVLT^{Vgat} and SFO^{Vglut2} neurons in the PVH and LT (Figure 3g-i). The density of collateral projections was lower than that of the projections to the SON, suggesting that only a subset of SON-projecting MnPO/OVLT^{Vglut2}, MnPO/OVLT^{Vgat} and SFO^{Vglut2} neurons send collaterals to the PVH and LT. Interestingly, we found that MnPO/OVLT-projecting SFO^{Vglut2} neurons, which include thirst-promoting neurons (Matsuda et al., 2017; Augustine et al., 2018), send a similar density of rabies-labeled fibers to the MnPO/OVLT, PVH and SON (Figure 3j). This result suggests that a majority of these SON-projecting SFO^{Vglut2} neurons send collaterals to the MnPO/OVLT and PVH, and, therefore may be capable of

simultaneously regulating AVP release and thirst. Together, these results indicate that, unlike convergence of afferent presystemic inputs to the MnPO/OVLT, downstream projections of the LT are redundantly organized such that presystemic information is shared not only between the LT structures but also between PVH^{AVP} and SON^{AVP} neurons via collateral projections.

SON-projecting LT neurons show presystemic responses to water-predicting cues and drinking

Next, we measured *in vivo* calcium dynamics of SON-projecting MnPO/OVLT and SFO neurons in response to water bowl presentation and drinking. GCaMP6s was expressed in SON-projecting excitatory or inhibitory neurons of the MnPO/OVLT and SFO using a modified herpes simplex virus that cre-dependently expresses GCaMP6s (HSV-GCaMP6s) and retrogradely infects neurons from the axon terminals (Kohl et al., 2018). HSV-GCaMP6s was injected into the SON of *Vglut2-IRES-Cre* or *Vgat-IRES-Cre* mice and an optic fiber was placed above the MnPO/OVLT or SFO (Figure 4a,g). We found that SON-projecting $MnPO/OVLT^{Vglut2}$ and SFO^{Vglut2} neurons both showed an immediate drop in activity upon water bowl placement (Figure 4b-e). A further drop in activity was observed as drinking continued. This resembled the response of SON^{AVP} neurons, suggesting that the inputs from $MnPO/OVLT^{Vglut2}$ and SFO^{Vglut2} neurons contribute to water-related presystemic regulation of AVP neurons. $MnPO/OVLT^{Vglut2}$ neurons showed a larger and sharper decrease in activity compared to SFO^{Vglut2} neurons when normalized values were compared (Figure 4f). Activity of

MnPO/OVLT^{Vglut2} neurons reached <50% of baseline activity within the first 1 min of drinking, whereas SFO^{Vglut2} neurons showed a gradual decrease that continued for over 5 min. A sharper drop in MnPO/OVLT^{Vglut2} neuron activity is consistent with significant attenuation of water-related presystemic response by MnPO, but not SFO, inhibition.

The SON-projecting MnPO/OVLT^{Vgat} neurons showed a completely different response (Figure 4h-k). Placement of the water bowl caused an abrupt increase in MnPO/OVLT^{Vgat} neuron activity, which rapidly declined and returned to baseline within 1 min. No drinking-related, long-term responses were observed. We hypothesize that SON-projecting MnPO/OVLT^{Vgat} neurons mainly signal the anticipation of water and work in parallel with MnPO/OVLT^{Vglut2} and SFO^{Vglut2} neurons to ensure rapid inhibition of AVP neuron activity upon water bowl placement. Together, these data indicate that the MnPO/OVLT is a key relay center for water-related presystemic information.

The LT does not mediate food-related presystemic regulation of AVP neurons

We found that the LT is involved in water-related presystemic regulation of SON^{AVP} neurons with the MnPO/OVLT playing a key role. We next tested whether the same region was involved in food-related presystemic regulation using the same approach as shown in Figure 2a. Mice were chronically food-restricted and were trained to take food pellets from a food bowl placed in the cage with varying latency. In the control group, as previously reported (Mandelblat-Cerf et al., 2017), SON^{AVP} neurons showed an increase in activity that began immediately upon feeding onset (Figure 5a). MnPO/OVLT inhibition did not affect the baseline activity (not shown) or

feeding-induced activation (Figure 5a-c). These results demonstrate that food-related presystemic regulation is mediated by a different circuit that does not involve the MnPO/OVLT.

We then explored the activity of SON-projecting LT neurons during food intake. In line with the result from MnPO/OVLT inhibition, none of the SON-projecting LT neurons displayed responses that could account for feeding-induced activation observed in SON^{AVP} neurons (Figure 5d,e). SON-projecting SFO^{Vglut2} and $MnPO/OVLT^{Vglut2}$ neurons showed an overall decrease in activity after food presentation but no consistent pattern was observed. SON-projecting $MnPO/OVLT^{Vgat}$ neurons were activated by food presentation but their activity gradually declined following feeding onset. Amplitude of these responses was significantly smaller than water-related responses of the same neurons (Figure 5e).

Presystemic activation of SON^{AVP} neurons is time-locked to the feeding onset (this study and (Mandelblat-Cerf et al., 2017)). To better compare responses in the LT neuron responses and in SON^{AVP} neurons, we reanalyzed the data by aligning the traces to feeding onset. SON-projecting SFO^{Vglut2}, $MnPO/OVLT^{Vglut2}$, and $MnPO/OVLT^{Vgat}$ neurons all showed a decrease in activity (Figure 5f). Even if these were to be bona fide responses, a small, simultaneous decrease in excitatory and inhibitory tone is unlikely to be the primary cause of rapid feeding-induced activation of SON^{AVP} neurons.

A previous study demonstrated rapid net activation of all excitatory SFO neurons by food intake (Zimmerman et al., 2016), which contradicts our finding. To resolve this

inconsistency, we performed fiber photometry from the entire SFO^{Vglut2} population. When compared to SON^{AVP} neurons, the response of SFO^{Vglut2} neurons was significantly delayed and lacked an early post-ingestive component occurring within 1 min of feeding onset (Figure 5g). Together, these results demonstrate that MnPO/OVLT and SFO are not involved in presystemic feeding-induced activation of SON^{AVP} neurons, supporting our finding that food- and water-related presystemic regulation is mediated by non-overlapping neural circuits.

Brainstem inputs do not mediate feeding-induced activation of AVP neurons

Given that the LT appears not to be involved in food-related presystemic regulation, we investigated other possible afferents that might provide food-related presystemic information to SON^{AVP} neurons. Due to inefficiency and tropism of the rabies virus, rabies retrograde tracing can, in some cases, be prone to false-negative results (Saleeba et al., 2019). Therefore, we decided to study additional sites suggested by a study using a traditional retrograde tracer (Tribollet et al., 1985): the nucleus of the solitary tract (NTS) and A1/C1 neurons in the ventrolateral medulla (VLM). Assuming that our rabies study failed to detect these afferents, we decided to investigate whether any of these areas provide direct inputs to AVP neurons. Catecholaminergic and glutamatergic input from A1/C1 neurons to AVP neurons have been validated in previous studies (Leng et al., 1999; Guyenet et al., 2013) and therefore their connection was not tested in our study. First, we explored the projections of NTS neurons using cre-independent ChR2 (AAV-ChR2-mCherry). Projections from the NTS were extremely

sparse in the PVH and nearly absent in the SON (Figure 6a,b). Subsequent CRACM showed that the NTS do not provide direct synaptic input to AVP neurons (Figure 6c). Similar results were obtained when A2 and excitatory neurons of the NTS were studied separately (Figure 6—figure supplement 1), and thus the NTS was not investigated further.

To test the involvement of A1/C1 neurons in food-related presystemic regulation, we inhibited A1/C1 neurons with hM4Di while monitoring *in vivo* calcium dynamics of SON^{AVP} neurons. In order to achieve specific expression of hM4Di in A1/C1 neurons, we used *AVP-IRES-Cre;DBH-Flp* mice in combination with a flp-dependent hM4Di virus (AAV-fDIO-hM4Di-mCherry) (Figure 6d). First, to test the effectiveness of hM4Di in silencing A1/C1 neurons, we studied the effect of CNO on hypotension-induced activation of AVP neurons. A1/C1 neurons are suggested to be crucial for hypotension-induced AVP release as non-specific inhibition/lesion of the VLM causes a significant attenuation of this response (Blessing and Willoughby, 1985; Head et al., 1987). A1/C1 inhibition significantly attenuated the activation of SON^{AVP} neurons in response to drug-induced hypotension (Figure 6e,f). This finding validates our experimental system and provides further evidence for the importance of A1/C1 neurons in hypotension-induced AVP release. We then used the same approach to examine the involvement of A1/C1 neurons in food-related presystemic regulation. In contrast to the robust blockade of hypotension-induced SON^{AVP} neuron activation, A1/C1 neuron inhibition had no effect on feeding-induced activation of SON^{AVP} neurons (Figure 6g,h). Together, these data indicate that blood pressure regulation is mediated by a circuit involving A1/C1 neurons and this circuit is distinct from the food-related presystemic circuit.

AgRP, POMC, and PNZ neurons do not mediate food-related presystemic regulation of AVP neurons

Next, we decided to test other afferents identified by rabies tracing – i.e. those coming from the ARC and PNZ (Figure 7a, Figure 7—figure supplement 1a). We first decided to focus on two genetically-accessible, functionally-relevant neuronal populations in the ARC, AgRP and POMC neurons, which have opposite roles in regulating food intake and energy balance. To investigate whether AgRP and POMC neurons provide direct inputs to PVH^{AVP} and SON^{AVP} neurons, we performed projection mapping and CRACM. AgRP and POMC projections were present in the PVH and SON but no synaptic connections were detected between AgRP/POMC and AVP neurons (Figure 7—figure supplement 2). In line with this, specific chemogenetic inhibition of AgRP or POMC neurons had no effect on the food-related presystemic response of SON^{AVP} neurons when investigated using fiber photometry in *AVP-IRES-Cre;AgRP/POMC-IRES-Cre* mice (Figure 7b-d). Short-term (<30 min following CNO injection) feeding behavior was not altered by AgRP or POMC neuron inhibition (Figure 7—figure supplement 3 and (Krashes et al., 2011; Uner et al., 2019)).

Another candidate input identified by rabies mapping is the PNZ (Figure 7—figure supplement 1a). GABAergic neurons in the PNZ (PNZ^{Vgat}) are believed to be involved in hypertension- and hypervolemia-induced inhibition of SON^{AVP} neurons (Grindstaff and Cunningham, 2001b, a; Cunningham et al., 2002). While we found that PNZ^{Vgat} neurons provided direct inhibitory input to AVP neurons and showed a selective

response to food but not water (Figure 7—figure supplement 1b-f), inhibition of these neurons had no effect on the baseline activity of SON^{AVP} neurons (not shown) or their response to feeding (Figure 7—figure supplement 1g-i). Together, these data suggest that AgRP, POMC, and PNZ^{Vgat} neurons are not primary contributors to food-related presystemic regulation.

Food-related presystemic regulation of AVP neurons is mediated by unknown neurons in the ARC

Next, we decided to focus on the entire ARC population. Because it is difficult to selectively target all ARC neurons without hitting surrounding nuclei, to examine the role of ARC neurons we decided to use a subtractive approach by creating three groups of animals with differing hM4Di expression: 1) ARC + VMH + DMH (Figure 7e), 2) VMH only (Figure 7i), and 3) DMH only (Figure 7k). This approach allowed for effective silencing of the ARC with hM4Di, which is difficult to achieve with restricted injection of cre-independent AAVs into the ARC. All three groups of mice underwent the same experimental protocol. Mice were chronically food-restricted and were habituated to the experimental session as described above. Inhibition of neurons in all three nuclei (ARC+VMH+DMH) caused a significant attenuation of feeding-induced activation that persisted throughout the recording (Figure 7f-h). In contrast, inhibition of the VMH (Figure 7j) or DMH (Figure 7l) alone, fully sparing the ARC, had no effect. Injection of CNO in all three groups did not affect the baseline activity of SON^{AVP} neurons (not shown). Together, these results indicate that the ARC contains a cell type, distinct from

AgRP or POMC neurons, that relay food-related presystemic signals to SON^{AVP} neurons.

Discussion

Water homeostasis is achieved by an intricate balance between water intake and output that are dictated, respectively, by thirst and antidiuretic hormone (AVP). While the field has experienced great advances in the neurobiological understanding of thirst in the last several years, our knowledge of neural regulation of AVP release remains rudimentary due to lack of technical approaches to reliably and temporally-precisely measure circulating AVP *in vivo*. In a prior study, by directly monitoring the activity of magnocellular AVP neurons, we demonstrated that AVP neuron activity, and thus likely AVP release, is altered surprisingly rapidly by water and food ingestion before any change in systemic osmolality is observed (Mandelblat-Cerf et al., 2017). While such feedforward, presystemic regulation has been demonstrated in other homeostatic circuits, AVP neurons are unique in that they are capable of responding to both water and food, and the response is *bidirectional* – water-predicting cues and drinking inhibit and eating activates AVP neurons – and *asymmetric* – water causes pre- and post-ingestive presystemic inhibition but food only causes post-ingestive presystemic activation. In this study, we expand on our prior findings by presenting a neural circuit mechanism by which these unique properties arise. Our study revealed two parallel, non-overlapping neural pathways for water- and food-related presystemic regulation (Table 1). Key components of the water-related presystemic circuit are neurons in the

LT, which provide direct synaptic input to AVP neurons and exhibit water-related presystemic responses that closely resemble those of AVP neurons. Food-related presystemic regulation, on the other hand, is mediated by an as yet unidentified neuronal population in the ARC that is completely distinct from feeding-regulating AgRP and POMC neurons. In the course of our study, we confirmed additional afferents that were previously proposed to be involved in other aspects of AVP function, such as A1/C1 neurons in the brainstem that mediate hypotension-induced AVP release (Blessing and Willoughby, 1985; Head et al., 1987; Leng et al., 1999; Guyenet et al., 2013). Collectively, these findings demonstrate that water- versus food-related presystemic signals are relayed to AVP neurons independently and differently via two non-overlapping circuits to give rise to the bidirectional, asymmetric presystemic response of AVP neurons.

Recent studies have identified multiple molecularly- or anatomically-distinct neuronal populations in the LT that are involved in different aspects of water homeostasis (Oka et al., 2015b; Abbott et al., 2016; Allen et al., 2017; Matsuda et al., 2017; Augustine et al., 2018; Pool et al., 2020). In this study, we investigated the role of the LT neurons in mediating presystemic regulation of AVP neurons. We identified at least three groups of LT neurons that provide direct input to AVP neurons: SFO^{Vglut2}, $MnPO/OVLT^{Vglut2}$ and $MnPO/OVLT^{Vgat}$ neurons. Interestingly, while all these neurons connect to AVP neurons with high probability, only MnPO/OVLT neurons were required for presystemic regulation. Remarkably, while mediating water-related presystemic responses, they played no role in mediating food-related presystemic responses. Thus, presystemic regulation of AVP neurons involves two distinct neural pathways dedicated

423 to water- or food-related regulation. Three groups of AVP-regulating LT neurons were
424 studied individually by selectively isolating them using projection-specific approaches
425 (i.e. to the SON) and genetic markers (i.e., *Vglut2* and *Vgat*). As can be expected from
426 their opposite neurochemical nature, SON-projecting MnPO/OVLT^{Vglut2} and
427 MnPO/OVLT^{Vgat} neurons showed opposing responses to water-related presystemic
428 signals. SON-projecting MnPO/OVLT^{Vglut2} neurons were rapidly suppressed by water-
429 predicting cues and drinking. This response nearly perfectly mirrored that of AVP
430 neurons suggesting that the decrease in SON-projecting MnPO/OVLT^{Vglut2} neuron
431 activity is a major cause of pre- and post-ingestive presystemic suppression of AVP
432 neurons. SON-projecting MnPO/OVLT^{Vgat} neurons, on the other hand, showed a brief
433 cue-induced activation, which likely functions to potentiate pre-ingestive inhibition of
434 AVP neurons. SON-projecting SFO^{Vglut2} neurons also showed presystemic suppression
435 but their contribution to presystemic regulation may be minor as inhibition of the SFO
436 did not affect the AVP neuron response. Of note, while we refer to SON-projecting LT
437 neurons as 'AVP-regulating' based on their high probability connections to SON^{AVP}
438 neurons, we acknowledge that subsets of SON-projecting LT neurons may also be
439 involved in regulation of other processes such as oxytocin release (via their connection
440 to SON^{Oxytocin} (non-AVP) neurons as demonstrated by CRACM) and thirst (via their
441 collaterals to other downstream structures as demonstrated by collateral mapping).

442 Presystemic responses of thirst-regulating counterparts of the LT has been
443 extensively studied by many groups (Zimmerman et al., 2016; Allen et al., 2017;
444 Augustine et al., 2018; Augustine et al., 2019; Zimmerman et al., 2019). While thirst-
445 regulating LT neurons also exhibit presystemic suppression (thirst-promoting neurons)

and activation (thirst-suppressing neurons), their responses surprisingly lack a pre-ingestive component that is present in AVP-regulating LT neurons and also hunger-regulating AgRP and POMC neurons (this study and (Betley et al., 2015; Chen et al., 2015; Mandelblat-Cerf et al., 2015)). This raises the possibility that presystemic regulation of thirst neurons may be different. Alternatively, it is possible that prior studies missed this regulation due to either its magnitude being small in comparison to post-ingestive regulation and/or the fact that population recordings, which may have pooled thirst-regulating LT neurons with other neurons, obscured its detection. In addition, considering that the pre-ingestive response is not innate but requires several days of training (Figure 2—figure supplement 1 and (Mandelblat-Cerf et al., 2017)), failure to detect pre-ingestive responses in these thirst-related studies might possibly be due to use of experimental paradigms not optimally designed to assess pre-ingestive responses.

The MnPO is traditionally considered as a hub that functions as the main input and output region of the LT (McKinley et al., 2015). In line with this, we found that SON-projecting MnPO/OVLT ^{Vglut2} neurons receive inputs from multiple regions outside the LT while inputs to SON-projecting SFO^{Vglut2} neurons were confined to the MnPO/OVLT. This result supports hierarchical organization of the LT with the MnPO/OVLT functioning as the main entry point for neurally transmitted afferent information. Systemic osmolality information (from the circumventricular organs (the SFO and OVLT)) and water-related presystemic information (from yet-undefined regions outside the LT) converge on the MnPO/OVLT and are redistributed to AVP neurons and other downstream targets directly, or indirectly via the SFO. Based on our rabies mapping of afferents to SON-

projecting MnPO/OVLT^{Vglut2} neurons, the following sites could in principle relay water-related presystemic information to the MnPO/OVLT: the VMH, DMH, PVH and LPBN. The DMH is of particular interest as it is already known to play a role in presystemic regulation of AgRP neurons (Garfield et al., 2016). By analogy, it may also contain neurons involved in water-related presystemic regulation of MnPO/OVLT neurons. The LPBN is also of interest in that it is known to relay interoceptive information to forebrain sites (Herbert et al., 1990), and it has been strongly implicated in regulation of water balance (Davern, 2014; Gizowski and Bourque, 2018). Indeed, recent studies identified two groups of thirst-suppressing neurons in the PBN that send direct projections to the MnPO/OVLT and exhibit post-ingestive activation in response to drinking (Ryan et al., 2017; Kim et al., 2020).

We found that food-related presystemic regulation is not mediated by the LT. LT neurons do not show food-related presystemic changes in their activity, and LT neuron inhibition does not affect food-related presystemic changes in AVP neuron activity. Inhibition of neurons in the ARC, on the other hand, causes a significant attenuation of food-related presystemic responses suggesting that neurons in the ARC mediate this regulation. Many anatomical and electrophysiological studies have demonstrated that AVP neurons receive direct excitatory and inhibitory projections from the ARC (Iijima and Ogawa, 1981; Saphier and Feldman, 1986; Leng et al., 1988; Ludwig and Leng, 2000; Pineda et al., 2016). This is further supported by our rabies mapping results. Due to technical limitations, however, the ARC neurons responsible for food-related presystemic regulation were not identified. The most widely-studied neurons in the ARC, AgRP and POMC neurons, were ruled out, as inhibition of these neurons had no effect

on the food-related presystemic response. Considering rapid feeding-induced activation of AVP neurons, it is highly likely that feeding-related presystemic regulation involves glutamatergic neurons in the ARC. Oxytocin receptor-expressing glutamatergic neurons (Fenselau et al., 2017) are a good candidate to mediate food-related presystemic regulation as these neurons are activated by feeding and are capable of inhibiting food intake rapidly when activated. Alternatively, it is possible that a completely novel ARC neuron is involved (Campbell et al., 2017). The combination of projection- and synaptic connectivity-based gene profiling techniques will facilitate specific identification of ARC neurons mediating food-related presystemic regulation.

In summary, presystemic regulation of AVP release is mediated by the LT and ARC circuits that, respectively, exclusively relay water- or food-related presystemic signals. The two circuits operate largely independently and relay different combinations of presystemic signals (water-related pre- and post-ingestive signals by the LT and food-related post-ingestive signals by the ARC), giving rise to the bidirectional and asymmetric nature of AVP neurons' presystemic responses. Additional anatomically and functionally distinct neural circuits converge on AVP neurons to mediate other aspects of AVP function, such as occurs during hypotension. Convergence and integration of multiple inputs at the level of AVP neurons, the final common pathway for AVP release, provide a neural circuit basis for differential regulation of AVP release by diverse behavioral and physiological stimuli. Identifying and characterizing key neural components of the extended neural circuitry underlying these processes will be an important area for future investigation.

514

515 Author Contributions

516 A.K., B.B.L., and M.L.A. conceived the studies. A.K. and J.C.M. conducted the studies.
517 C.W. generated AAV-nEf-fDIO-hM4Di-mCherry construct. A.K. and B.B.L. wrote the
518 manuscript with comments from all of the authors.

519

520 Acknowledgements

521 We would like to thank Drs. C. Saper, J. Majzoub, S. Liberles for helpful discussion; Y.
522 Li and Z. Yang for technical assistance; J. Lawitts at the BIDMC Transgenic Core; C.
523 Wang and Y. Zhang at BCH Viral Core. This research was funded by NIH F31
524 DK109575 (A.K.), NIH R01 DK075632, R01 DK096010, R01 DK089044, R01
525 DK111401, P30 DK046200, and P30 DK057521 (B.B.L), NIH New Innovator Award
526 DP2 DK105570, R01 DK109930, McKnight Scholar Award, and Pew Scholar Award
527 (M.L.A.).

528

529 Declaration of Interests

530 The authors declare no competing interests.

531

532

Materials and Methods

Ethics

All animal care and experimental procedures were approved in advance by the National Institute of Health and Beth Israel Deaconess Medical Center Institutional Animal Care and Use Committee.

Mice

Animals were housed at 22°C–24°C on a 12:12 light/dark cycle (light cycle: 6:00 am to 6:00 pm) with standard mouse chow (Teklad F6 Rodent Diet 8664; Harlan Teklad) and water provided ad libitum, unless specified otherwise. Adult male and female mice (8-16 weeks old) were used for experiments. Mice were maintained on a mixed background. Transgenic mouse strains used: *AVP-IRES-Cre* (Pei et al., 2014), *Slc17a6-IRES-cre* (*Vglut2-IRES-cre*) (Vong et al., 2011) (Jackson Labs Stock 016963), *Slc32a1-IRES-Cre* (*Vgat-IRES-Cre*) (Vong et al., 2011) (Jackson Labs stock 016962), *Nos-1-IRES-cre* (Jackson Labs Stock 017526), *TH-Cre* (Savitt et al., 2005) (Jackson Labs Stock 008601), *DBH-flp* (MMRRC 041575), *AVP-GFP* (MMRRC 015858-UCD), *Slc32a1-2A-FlpO* (Vgat-flp) (Jackson Labs Stock 029591), *AgRP-IRES-Cre* (Tong et al., 2008) (Jackson Labs Stock 012899), *POMC-IRES-Cre* (Fenselau et al., 2017).

Recombinant adeno-associated viral (rAAV) vectors

553 The following viral vectors were used in this study: AAV8-FLEX-TVA-mCherry
554 (UNC Vector Core, Addgene 38044), AAV1-CAG-FLEX-RG (UNC Vector Core,
555 Addgene 48333), SADΔG–EGFP (EnvA) rabies (Salk Gene Transfer Targeting and
556 Therapeutics Core, Addgene 32635), AAV9-EF1α-DIO-ChR2(H134R)-mCherry (Penn
557 Vector Core, Addgene 20297), AAV8-EF1a-DIO-synaptophysin-YFP (MIT Vector Core),
558 AAV9-CAG-ChR2(H134R)-mCherry (Penn Vector Core, Addgene 100054), HSV-
559 hEF1a-LS1L-GCaMP6s (MGH Gene Delivery Technology Core, RN507), AAV1-Syn-
560 FLEX-GCaMP6s (Penn Vector Core, Addgene 100845), AAV1-Ef1a-DIO-EYFP (UNC
561 Vector Core, Addgene 27056), AAV8-hSyn-hM4Di-mCherry (UNC Vector Core,
562 Addgene 50479), AAV8-hSyn-DIO-hM4Di-mCherry (UNC Vector Core, Addgene 44362),
563 AAV8-nEF-fDIO-hM4Di-mCherry (Boston Children's Hospital Viral Core, Custom-made
564 vector (hM4Di-mCherry was cut from AAV8-hSyn-DIO-hM4Di-mCherry (Addgene 44362)
565 by AscI and NheI, and subcloned into pAAV-nEF Con/Fon hChR2(H134R)-EYFP
566 (Addgene 55644) into AscI and XbaI))

567

568 **Stereotaxic surgery and viral injections**

569 For viral injections, mice were anaesthetized with ketamine/xylazine (100 and
570 10 mg/kg, respectively, i.p.) and then placed in a stereotaxic apparatus (David Kopf
571 model 940). A pulled glass micropipette (20-40 µm diameter tip) was used for
572 stereotaxic injections of adeno-associated virus (AAV). Virus was injected into the
573 posterior pituitary (100 nl; AP: −3.0 mm; ML: ±0 mm; DV: -6.0 mm from bregma),
574 SON/PNZ (100 nl/side; AP: −0.65 mm; ML: ±1.25 mm; DV: -5.4 mm from bregma),

MnPO/OVLT (10 nl/depth; AP: +0.25 mm; ML: 0 mm; DV: -4.8, 4.5 mm from bregma), SFO (10 nl; AP: -0.6 mm; ML: 0 mm; DV: -2.6 mm from bregma), PVH (50 nl/side; AP: -0.75 mm; ML: ±0.3 mm; DV: -4.85 mm from bregma), DMH (50 nl/side; AP: -1.85 mm; ML: ±0.3 mm; DV: -5.2 mm from bregma), VMH (50 nl/side; AP: -1.6 mm; ML: ±0.4 mm; DV: -5.5 mm from bregma), or Arcuate (50 nl/side; AP: -1.5 mm; ML: ±0.25 mm; DV: -5.8 mm from bregma) by an air pressure system using picoliter air puffs through a solenoid valve (Clippard EV 24VDC) pulsed by a Grass S48 stimulator to control injection speed (40 nL/min). The pipette was removed 3 min post-injection followed by wound closure using tissue adhesive (3M Vetbond). For viral injections into the NTS and VLM, mice were placed into a stereotaxic apparatus with the head angled down at approximately 45°. An incision was made at the level of the cisterna magna, then skin and muscle were retracted to expose the dura mater covering the 4th ventricle. A 28-gauge needle was used to make an incision in the dura and allow access to the NTS and VLM. Virus was then injected into the NTS (10nl/side; AP: -0.2mm; ML: ±0.2mm; DV: -0.2mm from obex) VLM (50nl*2/side; AP: -0.3 and -0.6mm; ML: ±1.3mm; DV: -1.7mm from obex) as described above. The pipette was removed 3 min post-injection followed by wound closure using absorbable suture for muscle and silk suture for skin. For fiber photometry, an optic fiber (200 µm diameter, NA=0.39, metal ferrule, Thorlabs) was implanted in the MnPO/OVLT, SFO, or SON and secured to the skull with dental cement. Subcutaneous injection of sustained release Meloxicam (4 mg/kg) was provided as postoperative care. The mouse was kept in a warm environment and closely monitored until resuming normal activity.

Brain slice electrophysiology and ChannelRhodopsin-assisted circuit mapping (CRACM)

To prepare brain slices for electrophysiological recordings, brains were removed from anesthetized mice and immediately placed in ice-cold cutting solution consisting of (in mM): 72 sucrose, 83 NaCl, 2.5 KCl, 1 NaH2PO4, 26 NaHCO3, 22 glucose, 5 MgCl2, 1 CaCl2, oxygenated with 95% O2 /5% CO2 , measured osmolarity 310-320 mOsm/l. Cutting solution was prepared and used within 72 hours. 250 µm-thick coronal sections containing the PVH and SON were cut with a vibratome (7000smz2-Campden Instruments) and incubated in oxygenated cutting solution at 34 °C for 25 min. The SON was located by using the bifurcation of the anterior and middle cerebral arteries on the ventral surface of the brain as a landmark. Slices were transferred to oxygenated aCSF (126 mM NaCl, 21.4 mM NaHCO3, 2.5 mM KCl, 1.2 mM NaH2PO4, 1.2 mM MgCl2, 2.4 mM CaCl2, 10 mM glucose) and stored in the same solution at room temperature (20-24 °C) for at least 60 min prior to recording. A single slice was placed in the recording chamber where it was continuously super-fused at a rate of 3–4 ml per min with oxygenated aCSF. Neurons were visualized with an upright microscope equipped with infrared-differential interference contrast and fluorescence optics. Borosilicate glass microelectrodes (5–7 MΩ) were filled with internal solution. Whole-cell voltage clamp recordings were obtained using Cs-based internal solutions containing either (in mM): 135 CsMeSO3, 10 HEPES, 1 EGTA, 4 MgCl2, 4 Na2-ATP, 0.4 Na2-GTP, 10 Na2-phosphocreatine (pH 7.3; 295 mOsm) for recording EPSCs; or for recording IPSCs

from Vgat neurons expressing ChR2: 140 CsCl, 1 BAPTA, 10 HEPES, 5 MgCl2, 5 Mg-ATP, 0.3 Na2GTP, and 10 lidocaine N-ethyl bromide (QX-314), pH 7.35 and 290 mOsm). To photostimulate ChR2-positive fibers, an LED light source (473 nm) was used. The blue light was focused on to the back aperture of the microscope objective, producing a wide-field exposure around the recorded cell of 1 mW. The light power at the specimen was measured using an optical power meter PM100D (ThorLabs). The light output is controlled by a programmable pulse stimulator, Master-8 (AMPI Co. Israel) and the pClamp 10.2 software (AXON Instruments). All recordings were made using Multiclamp 700B amplifier, and data was filtered at 2 kHz and digitized at 10 kHz. The photostimulation-evoked EPSC detection protocol consisted of four blue light laser pulses administered 1 s apart during the first 4 s of an 8 s sweep, repeated for a total of 30 sweeps. We attempted to maximize our ability to detect light-evoked currents by biasing our recordings to cell bodies within the densest axon fields. In some experiments, TTX (1 mM) and 4-AP (100 mM) was added to the bath solution in order to confirm monosynaptic connectivity. All CRACM results presented are from 2-3 mice per group. All analysis was conducted off-line in Clampfit 10 and Origin.

Fiber photometry experiments and analysis of photometry data

All experiments were conducted in the home-cage in freely moving mice. Beginning three weeks post-surgery (details above), animals prepared for *in vivo* fiber photometry experiments (outlined above), were food restricted to 85-90% of initial body weight. Over this one-week period, mice were acclimated to chow pellets (500mg, Bio-

Serv Dustless Precision Pellets), and to the food bowl and water bowl used in subsequent photometry experiments. Mice were habituated to the paradigm for at least 5 days prior to the first recording day. For experiments with hM4Di, saline or CNO (1mg/kg) was injected 20 min prior to the experiment. *In vivo* fiber photometry was conducted as previously described (Mandelblat-Cerf et al., 2017). A fiber optic cable (1-m long, metal ferrule, 400 µm diameter; Doric Lenses) was attached to the implanted optic cannula with zirconia sleeves (Doric Lenses). Laser light (473 nm) was focused on the opposite end of the fiber optic cable to titrate the light intensity entering the brain to 0.1-0.2 mW. Emitted light was passed through a dichroic mirror (Di02-R488-25x36, Semrock) and GFP emission filter (FF03-525/50-25, Semrock), before being focused onto a sensitive photodetector (Newport part #2151). The GCaMP6 signal was passed through a low-pass filter (50 Hz), and digitized at 1 KHz using a National Instruments data acquisition card and MATLAB software.

The recorded data was exported and then imported into MATLAB for analysis. Fluorescent traces were down-sampled to 1 Hz. We calculated the fractional change in GCaMP6s fluorescence according to the following equation: $\Delta F/F=(F - F0)/F0$, where F is fluorescence measurement and F0 is the mean fluorescence in the 30 sec prior to food/water bowl presentation or feeding onset or 2 or 3 min prior to drug injection. In some experiments, to facilitate the comparison across different groups, we normalized the responses of each mouse. In Fig. 4f, normalization was performed by $(\Delta F/F)/F_{total\Delta F}$, where $F_{total\Delta F}$ was maximum average change over the entire recording period. In Fig. 7e-l, normalization was performed by $(\Delta F/F)/F_{max\Delta F/F,control}$, where $F_{max\Delta F/F,control}$ was maximum average response of control trials within 5 min of feeding onset.

664

665 **Brain tissue preparation**

666 Animals were terminally anesthetized with 7% chloral hydrate diluted in saline
667 (350 mg/kg) and transcardially perfused with phosphate- buffered saline (PBS) followed
668 by 10% neutral buffered formalin (PFA). Brains were removed, stored in the same
669 fixative overnight, transferred into 20% sucrose at 4 °C overnight, and cut into 40- µm
670 sections on a freezing microtome (Leica) coronally into two equal series.

671

672 **Immunohistochemistry**

673 Brain sections were washed in PBS with Tween-20, pH 7.4 (PBST) and blocked
674 in 3% normal donkey serum in PBST for 1 h at room temperature. Brain sections were
675 then incubated overnight at room temperature in blocking solution containing primary
676 antiserum (rat anti-mCherry, Life Technologies M11217, 1:1,000; rabbit anti-dsRed,
677 Clontech 632496, 1:1,000; chicken anti-GFP, Life Technologies A10262, 1:1,000; rabbit
678 anti-vasopressin, Sigma-Aldrich AB1565, 1:1,000; rabbit anti-TH, Millipore AB152,
679 1:1,000; rabbit anti-POMC precursor, Phoenix Pharmaceuticals H-029-30, 1:1,000; goat
680 anti-AgRP, Neuromics GT15023, 1:1,000; chicken anti-GFP, Life Technologies A10262,
681 1:1,000;). The next morning sections were extensively washed in PBS and then
682 incubated in Alexa-fluorophore secondary antibody (1:1,000) for 1 h at room
683 temperature. After several washes in PBS, sections were mounted on gelatin-coated
684 slides and fluorescence images were captured with Olympus VS120 slide scanner
685 microscope.

686

Statistical analysis

Statistical analyses were performed using SigmaPlot software. Electrophysiological traces were analyzed on Clamp fit 10 (Molecular Devices) and Origin (Origin Lab) software. No statistical method was used to predetermine sample size. Blinding methods were not used. All data presented met the assumptions of the statistical test employed. Specific statistical tests are specified in the figure legends. Animals were excluded from analysis if histological validation revealed poor or inaccurate reporter expression or inaccurate fiber placement unless otherwise noted. n values reflect the final number of validated animals per group included in the analysis.

References

Abbott, S.B., Machado, N.L., Geerling, J.C., and Saper, C.B. (2016). Reciprocal Control of Drinking Behavior by Median Preoptic Neurons in Mice. J Neurosci 36, 8228-8237.

Allen, W.E., DeNardo, L.A., Chen, M.Z., Liu, C.D., Loh, K.M., Fenno, L.E., Ramakrishnan, C., Deisseroth, K., and Luo, L. (2017). Thirst-associated preoptic neurons encode an aversive motivational drive. Science 357, 1149-1155.

Andermann, M.L., and Lowell, B.B. (2017). Toward a Wiring Diagram Understanding of Appetite Control. Neuron 95, 757-778.

Arnauld, E., and du Pont, J. (1982). Vasopressin release and firing of supraoptic neurosecretory neurones during drinking in the dehydrated monkey. Pflugers Arch 394, 195-201.

Augustine, V., Ebisu, H., Zhao, Y., Lee, S., Ho, B., Mizuno, G.O., Tian, L., and Oka, Y. (2019). Temporally and Spatially Distinct Thirst Satiation Signals. Neuron 103, 242-249 e244.

Augustine, V., Gokce, S.K., Lee, S., Wang, B., Davidson, T.J., Reimann, F., Gribble, F., Deisseroth, K., Lois, C., and Oka, Y. (2018). Hierarchical neural architecture underlying thirst regulation. Nature 555, 204-209.

Augustine, V., Lee, S., and Oka, Y. (2020). Neural Control and Modulation of Thirst, Sodium Appetite, and Hunger. Cell 180, 25-32.

Betley, J.N., Cao, Z.F., Ritola, K.D., and Sternson, S.M. (2013). Parallel, redundant circuit organization for homeostatic control of feeding behavior. Cell 155, 1337-1350.

Betley, J.N., Xu, S., Cao, Z.F., Gong, R., Magnus, C.J., Yu, Y., and Sternson, S.M. (2015). Neurons for hunger and thirst transmit a negative-valence teaching signal. Nature.

Blair-West, J.R., Gibson, A.P., Woods, R.L., and Brook, A.H. (1985). Acute reduction of plasma vasopressin levels by rehydration in sheep. Am J Physiol 248, R68-71.

Blessing, W.W., and Willoughby, J.O. (1985). Inhibiting the rabbit caudal ventrolateral medulla prevents baroreceptor-initiated secretion of vasopressin. J Physiol 367, 253-265.

Bolignano, D., Cabassi, A., Fiaccadori, E., Ghigo, E., Pasquali, R., Peracino, A., Peri, A., Plebani, M., Santoro, A., Settanni, F., and Zoccali, C. (2014). Copeptin (CTproAVP), a new tool for understanding the role of vasopressin in pathophysiology. Clin Chem Lab Med 52, 1447-1456.

740 Brown, C.H., Bains, J.S., Ludwig, M., and Stern, J.E. (2013). Physiological regulation of
741 magnocellular neurosecretory cell activity: integration of intrinsic, local and afferent
742 mechanisms. J Neuroendocrinol 25, 678-710.

743 Campbell, J.N., Macosko, E.Z., Fenselau, H., Pers, T.H., Lyubetskaya, A., Tenen, D.,
744 Goldman, M., Verstegen, A.M., Resch, J.M., McCarroll, S.A.*, et al.* (2017). A molecular
745 census of arcuate hypothalamus and median eminence cell types. Nat Neurosci 20,
746 484-496.

747 Choudhury, S.R., and Ray, P.K. (1990). Ultrastructural features of presumptive
748 vasopressinergic synapses in the hypothalamic magnocellular secretory nuclei of the rat.
749 Acta Anat (Basel) 137, 252-256.

750 Christ-Crain, M., and Fenske, W. (2016). Copeptin in the diagnosis of vasopressin-
751 dependent disorders of fluid homeostasis. Nat Rev Endocrinol 12, 168-176.

752 Cunningham, J.T., Bruno, S.B., Grindstaff, R.R., Grindstaff, R.J., Higgs, K.H., Mazzella,
753 D., and Sullivan, M.J. (2002). Cardiovascular regulation of supraoptic vasopressin
754 neurons. Prog Brain Res 139, 257-273.

755 Davern, P.J. (2014). A role for the lateral parabrachial nucleus in cardiovascular
756 function and fluid homeostasis. Front Physiol 5, 436.

757 Fenselau, H., Campbell, J.N., Verstegen, A.M., Madara, J.C., Xu, J., Shah, B.P., Resch,
758 J.M., Yang, Z., Mandelblat-Cerf, Y., Livneh, Y., and Lowell, B.B. (2017). A rapidly acting
759 glutamatergic ARC-->PVH satiety circuit postsynaptically regulated by alpha-MSH. Nat
760 Neurosci 20, 42-51.

761 Ferguson, J.W., Therapondos, G., Newby, D.E., and Hayes, P.C. (2003). Therapeutic
762 role of vasopressin receptor antagonism in patients with liver cirrhosis. Clin Sci (Lond)
763 105, 1-8.

764 Garfield, A.S., Shah, B.P., Burgess, C.R., Li, M.M., Li, C., Steger, J.S., Madara, J.C.,
765 Campbell, J.N., Kroeger, D., Scammell, T.E.*, et al.* (2016). Dynamic GABAergic afferent
766 modulation of AgRP neurons. Nat Neurosci 19, 1628-1635.

767 Geelen, G., Keil, L.C., Kravik, S.E., Wade, C.E., Thrasher, T.N., Barnes, P.R., Pyka, G.,
768 Nesvig, C., and Greenleaf, J.E. (1984). Inhibition of plasma vasopressin after drinking in
769 dehydrated humans. Am J Physiol 247, R968-971.

770 Gizowski, C., and Bourque, C.W. (2018). The neural basis of homeostatic and
771 anticipatory thirst. Nat Rev Nephrol 14, 11-25.

772 Grindstaff, R.R., and Cunningham, J.T. (2001a). Cardiovascular regulation of
773 vasopressin neurons in the supraoptic nucleus. Exp Neurol 171, 219-226.

774 Grindstaff, R.R., and Cunningham, J.T. (2001b). Lesion of the perinuclear zone
775 attenuates cardiac sensitivity of vasopressinergic supraoptic neurons. Am J Physiol
776 Regul Integr Comp Physiol 280, R630-638.

777 Guyenet, P.G., Stornetta, R.L., Bochorishvili, G., Depuy, S.D., Burke, P.G., and Abbott,
778 S.B. (2013). C1 neurons: the body's EMTs. Am J Physiol Regul Integr Comp Physiol
779 305, R187-204.

780 Head, G.A., Quail, A.W., and Woods, R.L. (1987). Lesions of A1 noradrenergic cells
781 affect AVP release and heart rate during hemorrhage. Am J Physiol 253, H1012-1017.

782 Herbert, H., Moga, M.M., and Saper, C.B. (1990). Connections of the parabrachial
783 nucleus with the nucleus of the solitary tract and the medullary reticular formation in the
784 rat. J Comp Neurol 293, 540-580.

785 Huang, W., Sved, A.F., and Stricker, E.M. (2000). Water ingestion provides an early
786 signal inhibiting osmotically stimulated vasopressin secretion in rats. Am J Physiol
787 Regul Integr Comp Physiol 279, R756-760.

788 Iijima, K., and Ogawa, T. (1981). An HRP study on the distribution of all nuclei
789 innervating the supraoptic nucleus in the rat brain. Acta Histochem 69, 274-295.

790 Kim, D.Y., Heo, G., Kim, M., Kim, H., Jin, J.A., Kim, H.K., Jung, S., An, M., Ahn, B.H.,
791 Park, J.H.*, et al.* (2020). A neural circuit mechanism for mechanosensory feedback
792 control of ingestion. Nature 580, 376-380.

793 Kohl, J., Babayan, B.M., Rubinstein, N.D., Autry, A.E., Marin-Rodriguez, B., Kapoor, V.,
794 Miyamishi, K., Zweifel, L.S., Luo, L., Uchida, N., and Dulac, C. (2018). Functional circuit
795 architecture underlying parental behaviour. Nature 556, 326-331.

796 Krashes, M.J., Koda, S., Ye, C., Rogan, S.C., Adams, A.C., Cusher, D.S., Maratos-Flier,
797 E., Roth, B.L., and Lowell, B.B. (2011). Rapid, reversible activation of AgRP neurons
798 drives feeding behavior in mice. J Clin Invest 121, 1424-1428.

799 Leib, D.E., Zimmerman, C.A., Poormoghaddam, A., Huey, E.L., Ahn, J.S., Lin, Y.C.,
800 Tan, C.L., Chen, Y.M., and Knight, Z.A. (2017). The Forebrain Thirst Circuit Drives
801 Drinking through Negative Reinforcement. Neuron 96, 1272-+.

802 Leng, G., Brown, C.H., and Russell, J.A. (1999). Physiological pathways regulating the
803 activity of magnocellular neurosecretory cells. Prog Neurobiol 57, 625-655.

804 Leng, G., Yamashita, H., Dyball, R.E., and Bunting, R. (1988). Electrophysiological
805 evidence for a projection from the arcuate nucleus to the supraoptic nucleus. Neurosci
806 Lett 89, 146-151.

807 Livneh, Y., Ramesh, R.N., Burgess, C.R., Levandowski, K.M., Madara, J.C., Fenselau,
808 H., Goldey, G.J., Diaz, V.E., Jikomes, N., Resch, J.M.*, et al.* (2017). Homeostatic
809 circuits selectively gate food cue responses in insular cortex. Nature 546, 611-616.

810 Livneh, Y., Sugden, A.U., Madara, J.C., Essner, R.A., Flores, V.I., Sugden, L.A., Resch,
811 J.M., Lowell, B.B., and Andermann, M.L. (2020). Estimation of Current and Future
812 Physiological States in Insular Cortex. Neuron.

813 Ludwig, M., and Leng, G. (2000). GABAergic projection from the arcuate nucleus to the
814 supraoptic nucleus in the rat. Neurosci Lett 281, 195-197.

815 Mandelblat-Cerf, Y., Kim, A., Burgess, C.R., Subramanian, S., Tannous, B.A., Lowell,
816 B.B., and Andermann, M.L. (2017). Bidirectional Anticipation of Future Osmotic
817 Challenges by Vasopressin Neurons. Neuron 93, 57-65.

818 Matsuda, T., Hiyama, T.Y., Niimura, F., Matsusaka, T., Fukamizu, A., Kobayashi, K.,
819 Kobayashi, K., and Noda, M. (2017). Distinct neural mechanisms for the control of thirst
820 and salt appetite in the subfornical organ. Nat Neurosci 20, 230-241.

821 McKinley, M.J., Mathai, M.L., McAllen, R.M., McClear, R.C., Miselis, R.R., Pennington,
822 G.L., Vivas, L., Wade, J.D., and Oldfield, B.J. (2004). Vasopressin secretion: osmotic
823 and hormonal regulation by the lamina terminalis. J Neuroendocrinol 16, 340-347.

824 McKinley, M.J., Yao, S.T., Uschakov, A., McAllen, R.M., Rundgren, M., and Martelli, D.
825 (2015). The median preoptic nucleus: front and centre for the regulation of body fluid,
826 sodium, temperature, sleep and cardiovascular homeostasis. Acta Physiol (Oxf) 214, 8-
827 32.

828 Nielsen, S., Chou, C.L., Marples, D., Christensen, E.I., Kishore, B.K., and Knepper, M.A.
829 (1995). Vasopressin increases water permeability of kidney collecting duct by inducing
830 translocation of aquaporin-CD water channels to plasma membrane. Proc Natl Acad Sci
831 U S A 92, 1013-1017.

832 Oka, Y., Ye, M., and Zuker, C.S. (2015a). Thirst driving and suppressing signals
833 encoded by distinct neural populations in the brain. Nature.

834 Oka, Y., Ye, M., and Zuker, C.S. (2015b). Thirst driving and suppressing signals
835 encoded by distinct neural populations in the brain. Nature 520, 349-352.

836 Pei, H., Sutton, A.K., Burnett, K.H., Fuller, P.M., and Olson, D.P. (2014). AVP neurons
837 in the paraventricular nucleus of the hypothalamus regulate feeding. Mol Metab 3, 209-
838 215.

839 Pineda, R., Sabatier, N., Ludwig, M., Millar, R.P., and Leng, G. (2016). A Direct
840 Neurokinin B Projection from the Arcuate Nucleus Regulates Magnocellular
841 Vasopressin Cells of the Supraoptic Nucleus. J Neuroendocrinol 28.

Pool, A.H., Wang, T., Stafford, D.A., Chance, R.K., Lee, S., Ngai, J., and Oka, Y. (2020). The cellular basis of distinct thirst modalities. Nature 588, 112-117.

Ryan, P.J., Ross, S.I., Campos, C.A., Derkach, V.A., and Palmiter, R.D. (2017). Oxytocin-receptor-expressing neurons in the parabrachial nucleus regulate fluid intake. Nat Neurosci 20, 1722-1733.

Saleeba, C., Dempsey, B., Le, S., Goodchild, A., and McMullan, S. (2019). A Student's Guide to Neural Circuit Tracing. Front Neurosci 13, 897.

Saphier, D., and Feldman, S. (1986). Electrophysiologic evidence for connections between the supraoptic and the arcuate/ventromedial hypothalamic nuclei in the rat. Exp Neurol 92, 563-570.

Savitt, J.M., Jang, S.S., Mu, W., Dawson, V.L., and Dawson, T.M. (2005). Bcl-x is required for proper development of the mouse substantia nigra. J Neurosci 25, 6721-6728.

Silverman, A.J., Hou-Yu, A., and Zimmerman, E.A. (1983). Ultrastructural studies of vasopressin neurons of the paraventricular nucleus of the hypothalamus using a monoclonal antibody to vasopressin: analysis of synaptic input. Neuroscience 9, 141-155.

Stricker, E.M., and Hoffmann, M.L. (2007). Presystemic signals in the control of thirst, salt appetite, and vasopressin secretion. Physiol Behav 91, 404-412.

Stricker, E.M., and Stricker, M.L. (2011). Pre-systemic controls of fluid intake and vasopressin secretion. Physiol Behav 103, 86-88.

Thrasher, T.N., Keil, L.C., and Ramsay, D.J. (1987). Drinking, oropharyngeal signals, and inhibition of vasopressin secretion in dogs. Am J Physiol 253, R509-515.

Thrasher, T.N., Nistal-Herrera, J.F., Keil, L.C., and Ramsay, D.J. (1981). Satiety and inhibition of vasopressin secretion after drinking in dehydrated dogs. Am J Physiol 240, E394-401.

Tong, Q., Ye, C.P., Jones, J.E., Elmquist, J.K., and Lowell, B.B. (2008). Synaptic release of GABA by AgRP neurons is required for normal regulation of energy balance. Nat Neurosci 11, 998-1000.

Tribollet, E., Armstrong, W.E., Dubois-Dauphin, M., and Dreifuss, J.J. (1985). Extra-hypothalamic afferent inputs to the supraoptic nucleus area of the rat as determined by retrograde and anterograde tracing techniques. Neuroscience 15, 135-148.

Uner, A.G., Kecik, O., Quaresma, P.G.F., De Araujo, T.M., Lee, H., Li, W., Kim, H.J., Chung, M., Bjorbaek, C., and Kim, Y.B. (2019). Role of POMC and AgRP neuronal activities on glycaemia in mice. Sci Rep 9, 13068.

877 Vong, L., Ye, C., Yang, Z., Choi, B., Chua, S., Jr., and Lowell, B.B. (2011). Leptin action
878 on GABAergic neurons prevents obesity and reduces inhibitory tone to POMC neurons.
879 Neuron 71, 142-154.

880 Zimmerman, C.A., Huey, E.L., Ahn, J.S., Beutler, L.R., Tan, C.L., Kosar, S., Bai, L.,
881 Chen, Y., Corpuz, T.V., Madisen, L.*, et al.* (2019). A gut-to-brain signal of fluid
882 osmolarity controls thirst satiation. Nature 568, 98-102.

883 Zimmerman, C.A., Lin, Y.C., Leib, D.E., Guo, L., Huey, E.L., Daly, G.E., Chen, Y., and
884 Knight, Z.A. (2016). Thirst neurons anticipate the homeostatic consequences of eating
885 and drinking. Nature 537, 680-684.

886

887

888

889

890

891

892

893

894

895

896

897

Figure Legends

Figure 1 Magnocellular AVP neurons receive excitatory and inhibitory input from the LT.

a, e, Schematic of monosynaptic rabies tracing from magnocellular PVH^{AVP} (a) and SON^{AVP} (e) neurons. In order to target magnocellular PVH^{AVP} neurons, rabies virus was injected into the posterior pituitary.

b, f, Representative images showing magnocellular PVH^{AVP} (c) and SON^{AVP} (f) starter neurons as identified by co-expression of GFP and mCherry.

c, g, Representative images showing magnocellular PVH^{AVP} (c) and SON^{AVP} (g) starter neurons and dense rabies labeling in the SON (c) and PVH (g).

d, h, Representative images showing sites containing rabies-labeled neurons in the LT that are monosynaptically connected to magnocellular PVH^{AVP} (d) and SON^{AVP} (h) neurons.

i, Schematic of anterograde tracing from excitatory and inhibitory neurons in the SFO and MnPO/OVLT.

j, Representative images showing expression of Syn-YFP in excitatory and inhibitory neurons in the SFO and MnPO/OVLT (left box), and their efferent projections in the SFO, MnPO, OVLT, PVH and SON (right box). Note lack of YFP-labeled fibers from SFO^{Vgat} neurons in the PVH and SON.

k, Schematic of CRACM (top) and representative images showing co-localization of GFP and AVP immunofluorescence (red) in the PVH (bottom left) and SON (bottom right) of AVP-GFP mice.

l, m, Number of PVH^{AVP} and SON^{AVP} neurons (l) and non-GFP PVH and SON neurons (m) receiving direct synaptic inputs from $MnPO/OVLT^{Vglut2}$, SFO^{Vglut2}, and $MnPO/OVLT^{Vgat}$ neurons as identified by CRACM. Mice used include *AVP-GFP;Vglut2-IRES-Cre* ($MnPO/OVLT^{Vglut2}$ and SFO^{Vglut2}) and *AVP-GFP;Vgat-IRES-Cre* ($MnPO/OVLT^{Vgat}$) Scale bar, 200µm.

n, Representative traces showing light-evoked responses in SFO^{Vglut2} to SON^{AVP} (left), $MnPO/OVLT^{Vglut2}$ to SON^{AVP} (middle), and $MnPO/OVLT^{Vgat}$ to SON^{AVP} (right) CRACM. Black trace is an average of all traces (gray) in consecutive trials.

Figure 2 The LT mediates water-related presystemic regulation of SON^{AVP} neurons.

a, i, Schematic of SON^{AVP} photometry experiment with hM4Di-mediated non-specific inhibition of neurons in the MnPO/OVLT (a) and SFO (i).

b, j, Single-trial timecourses of SON^{AVP} population activity in response to water bowl placement in saline and CNO trials of mice expressing hM4Di in the MnPO/OVLT (b) and SFO (j). Trials are sorted according to latency from water bowl placement to drinking onset (black ticks). n= 6 (MnPO), 5 (SFO) mice.

c, k, Average SON^{AVP} population activity in response to water bowl placement in saline and CNO trials of mice expressing hM4Di in the MnPO/OVLT (c) and SFO (k). n= 6 (MnPO), 5 (SFO) mice.

d, l, Average of pre-ingestive responses in saline and CNO trials of mice expressing hM4Di in the MnPO/OVLT (k) and SFO (l). n= 6 (MnPO), 5 (SFO) mice. Values are means ± SEMs across trials.

e, m, Data from panel c (e) and k (m) binned across drinking periods. ***$p < 0.001$; repeated measures (RM) 2-way ANOVA, n= 6 (MnPO), 5 (SFO) mice.

f, n, Average pre- and post-ingestive responses in saline and CNO trials of mice expressing hM4Di in the MnPO/OVLT (f) and SFO (n). ns, $p > 0.05$; *$p < 0.05$; **$p<0.01$; paired t-test, n= 6 (MnPO), 5 (SFO) mice.

g, o, Average latency to drinking onset and number of drinking bouts in saline and CNO trials of mice expressing hM4Di in the MnPO/OVLT (k) and SFO (l). ns, $p > 0.05$; *$p < 0.05$; **$p<0.01$; paired t-test, n= 6 (MnPO), 5 (SFO) mice.

h, p, Average change in baseline activity in saline and CNO trials of mice expressing hM4Di in the MnPO/OVLT (h) and SFO (p). ns, $p > 0.05$; *$p < 0.05$; **$p<0.01$; paired t-test, n= 6 (MnPO), 3 (SFO) mice.

Values are means ± SEMs across mice except for d, l.

See also Figure1-—figure supplement 1,2.

Figure 3 Organization of water-related presystemic neural circuit.

a, Schematic of monosynaptic rabies tracing from $MnPO/OVLT^{Vglut2}$ neurons.

b, c, Representative images showing $MnPO/OVLT^{Vglut2}$ starter neurons as identified by co-expression of GFP and mCherry (b), and sites containing rabies-labeled neurons that are monosynaptically connected to $MnPO/OVLT^{Vglut2}$ neurons (c).

d, Schematic of monosynaptic rabies tracing from SFO^{Vglut2} neurons.

e, f, Representative image showing SFO^{Vglut2} starter neurons as identified by co-expression of GFP and mCherry (e), and sites containing rabies-labeled neurons that are monosynaptically connected to SFO^{Vglut2} neurons (f).

g-j, Schematic of rabies-based axon collateral mapping (left), Representative images showing starter neurons (middle), and Rabies-labeled collateral projections (right) of SON-projecting MnPO/OVLT^{Vglut2} (g), MnPO/OVLT^{Vgat} (h), and SFO^{Vglut2} (i) neurons and MnPO/OVLT-projecting SFO^{Vglut2} (j) neurons.

Arrows, rabies-labeled collateral projections. Scale bar, 200µm.

See also Figure 3—figure supplement 1.

Figure 4 SON-projecting SFO^{Vglut2}, MnPO/OVLT^{Vglut2}, and MnPO/OVLT^{Vgat} neurons show presystemic responses to water bowl placement and drinking.

a, Schematic of photometry experiment from SON-projecting SFO^{Vglut2} and MnPO/OVLT^{Vglut2} neurons.

b, Single-trial timecourses of SON-projecting SFO^{Vglut2} (top) and MnPO/OVLT^{Vglut2} (bottom) population activity in response to water bowl placement. Trials are sorted according to latency from water bowl placement to drinking onset (black ticks). n= 7 (SFO^{Vglut2}), and 5 (MnPO/OVLT^{Vglut2}) mice.

c, Average population activity of SON-projecting SFO^{Vglut2} (light blue) and MnPO/OVLT^{Vglut2} (dark blue) neurons in response to water bowl placement. n= 7 (SFO^{Vglut2}), and 5 (MnPO/OVLT^{Vglut2}) mice.

d, Average pre-ingestive responses of SON-projecting SFO^{Vglut2} (light blue) and MnPO/OVLT^{Vglut2} (dark blue) neurons. n= 7 (SFO^{Vglut2}), and 5 (MnPO/OVLT^{Vglut2}) mice. Values are means ± SEMs across trials.

e, Data from panel c binned across drinking periods. n= 7 (SFO^{Vglut2}), and 5 (MnPO/OVLT^{Vglut2}) mice.

f, Normalized average SON-projecting SFO^{Vglut2} and MnPO/OVLT^{Vglut2} population activity binned across drinking periods. Values are normalized to the total change. ***p < 0.001; 2-way ANOVA, n= 7 (SFO^{Vglut2}), and 5 (MnPO/OVLT^{Vglut2}) mice.

g, Schematic of photometry experiment from SON-projecting MnPO/OVLT^{Vgat} neurons.

h, Single-trial timecourses of SON-projecting MnPO/OVLT^{Vgat} population activity in response to water bowl placement. Trials are sorted according to latency from water bowl placement to drinking onset (black ticks). n= 9 mice.

i, Average population activity of SON-projecting MnPO/OVLT^{Vgat} neurons in response to water bowl placement. n= 9 mice.

j, Average pre-ingestive responses of SON-projecting MnPO/OVLT^{Vgat} neurons. n= 9 mice. Values are means ± SEMs across trials.

k, Data from panel l binned across drinking periods. n= 9 mice.

Scale bar, 200µm. Values are means ± SEMs across mice except for d, j.

Figure 5 The MnPO/OVLT is not involved in food-related presystemic regulation of SON^{AVP} neurons.

a, Single-trial timecourses of SON^{AVP} population activity in response to food bowl placement in saline and CNO trials. Trials are sorted according to latency from food bowl placement to feeding onset (black ticks). n=5 mice.

b, Average population activity of SON^{AVP} neurons in response to feeding onset in saline and CNO trials. n=5 mice.

c, Data from panel b binned across feeding periods. n=5 mice.

d, Single-trial timecourses of SON-projecting SFO^{Vglut2}, MnPO/OVLT^{Vglut2}, and MnPO/OVLT^{Vgat} population activity in response to food bowl placement. Trials are sorted according to latency from food bowl placement to feeding onset (black ticks). n= 7 (SFO^{Vglut2}), and 5 (MnPO/OVLT^{Vglut2}), and 9 (MnPO/OVLT^{Vgat}) mice.

e, Average population response of SON-projecting SFO^{Vglut2}, MnPO/OVLT^{Vglut2}, and MnPO/OVLT^{Vgat} neurons to food bowl placement (top) and water (closed circles, solid line) versus food (open circles, dotted line) bowl placement (bottom).

f, Average population activity of SON-projecting SFO^{Vglut2}, MnPO/OVLT^{Vglut2}, and MnPO/OVLT^{Vgat} neurons aligned to feeding onset.

g, Average population activity of SON^{AVP}, SFO^{Vglut2}, and SON-projecting SFO^{Vglut2} neurons aligned to feeding onset. n= 5 (SON^{AVP}), 3 (SFO^{Vglut2}), and 7 (SON-projecting SFO^{Vglut2}) mice.

Values are means ± SEMs across mice.

Figure 6 Brainstem inputs do not mediate feeding-induced activation of SON^{AVP} neurons.

a, Representative images showing expression of ChR2-mCherry in the NTS (top), and their efferent projections in the PVH and SON (bottom).

b, Number of PVH^{AVP} and SON^{AVP} neurons (left), and non-GFP PVH and SON neurons (right) receiving direct synaptic inputs from the NTS.

c, Representative traces showing light-evoked responses. Black trace is an average of all traces (gray) in consecutive trials.

d, Schematic of SON^{AVP} photometry experiment with hM4Di-mediated inhibition of A1/C1 neurons.

e, Average SON^{AVP} population activity to hypotension induced by vasodilating drug HDZ in saline and CNO trials.

f, Data from panel e binned every 5 min. ***$p < 0.001$; RM 2-way ANOVA, n= 9 mice.

g, Average SON^{AVP} population activity in response to feeding onset in saline and CNO trials.

h, Data from panel g binned across feeding periods. ns, $p > 0.05$; RM 2-way ANOVA, n= 8 mice.

Scale bar, 500µm. Values are means ± SEMs across mice.

See also Figure 6—figure supplement 1.

Figure 7 non-AgRP/POMC neurons in the ARC mediate food-related presystemic regulation of SON^{AVP} neurons.

a, Representative image showing rabies-labeled neurons in the ARC that are monosynaptically connected to magnocellular SON^{AVP} neurons.

b, Schematic of SON^{AVP} photometry experiment with hM4Di-mediated inhibition of AgRP or POMC neurons.

c, Representative images showing hM4Di expression in AgRP (top) and POMC neurons (bottom).

d, Average SON^{AVP} population activity binned across feeding periods in saline and CNO trials of *AVP-IRES-Cre;Agrp-IRES-Cre* (top) and *AVP-IRES-Cre;Pomc-IRES-Cre* (bottom) mice.

e, i, k, Schematic of SON^{AVP} photometry experiment with hM4Di-mediated non-specific inhibition of the ARC+VMH+DMH (e), VMH only (i), and DMH only (k).

f, Single-trial timecourses of SON^{AVP} population activity in response to food bowl placement in saline and CNO trials of ARC+VMH+DMH group. Trials are sorted according to latency from food bowl placement to feeding onset (black ticks). n= 5 mice.

g, Average SON^{AVP} population activity in response to feeding onset in saline and CNO trials of ARC+VMH+DMH group. n= 9 mice.

h, j, l, Average SON^{AVP} population activity binned across feeding periods in saline and CNO trials of ARC+VMH+DMH (h), VMH only (j), and DMH only (l) groups. ns, $p > 0.05$; *$p < 0.05$; RM 2-way ANOVA, n= 5 (ARC+VMH+DMH), 4 (VMH only), 7 (DMH only) mice.

Scale bar, 200µm. Values are means ± SEMs across mice.

See also Figures 7—figure supplement 1-3.

1092 **Table 1 Summary of the result.**

1093

Afferents tested	Connection to AVP neurons (validation method)	Presystemic response (pre-/post -ingestive)		Effect of inhibition on AVP neuron activity
		Water	Food	
SON-projecting SFO^{Vglut2}, MnPO/OVLT^{Vglut2}	✓ (Rabies mapping, CRACM, projection mapping)	↓ / ↓↓	↔ / ↔	▼ Water-related presystemic response
SON-projecting MnPO/OVLT^{Vgat}	✓ (Rabies mapping, CRACM, projection mapping)	↑ / ↔	↑ / ↔	
A1/C1	✓ (CRACM, projection mapping)	?	?	▼ Hypotension-induced activation
PNZ^{Vgat}	✓ (Rabies mapping, CRACM)	↑ / ↔	↑ / ↓↓	No effect
AgRP[a]	X (Rabies mapping, CRACM, projection mapping)	↔	↓ / ↓↓	No effect
POMC[a]	X (Rabies mapping, CRACM, projection mapping)	?	↑ / ↑↑	No effect
ARC	✓ (Rabies mapping)	?	?	▼ Feeding-related presystemic response

1094 ✓, connected; X, not connected; ↑, increase (↑<↑↑); ↓, decrease (↓<↓↓); ↔, no change; ?, not
1095 tested; ▼, significantly attenuated; a, Betley et al., 2015; Chen et al., 2015; Mandelblat-Cerf et
1096 al., 2015

Figure 1

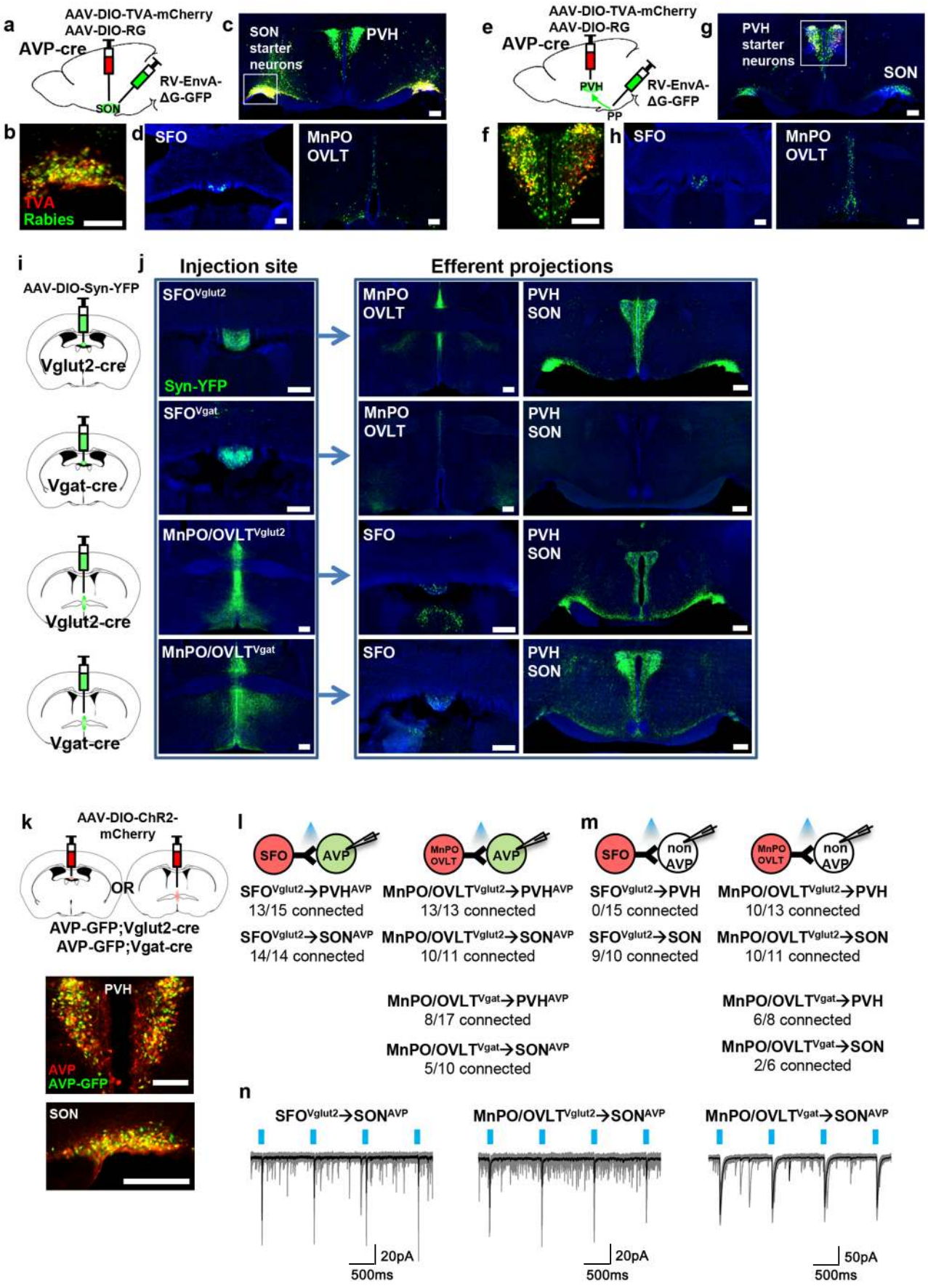

Figure 2

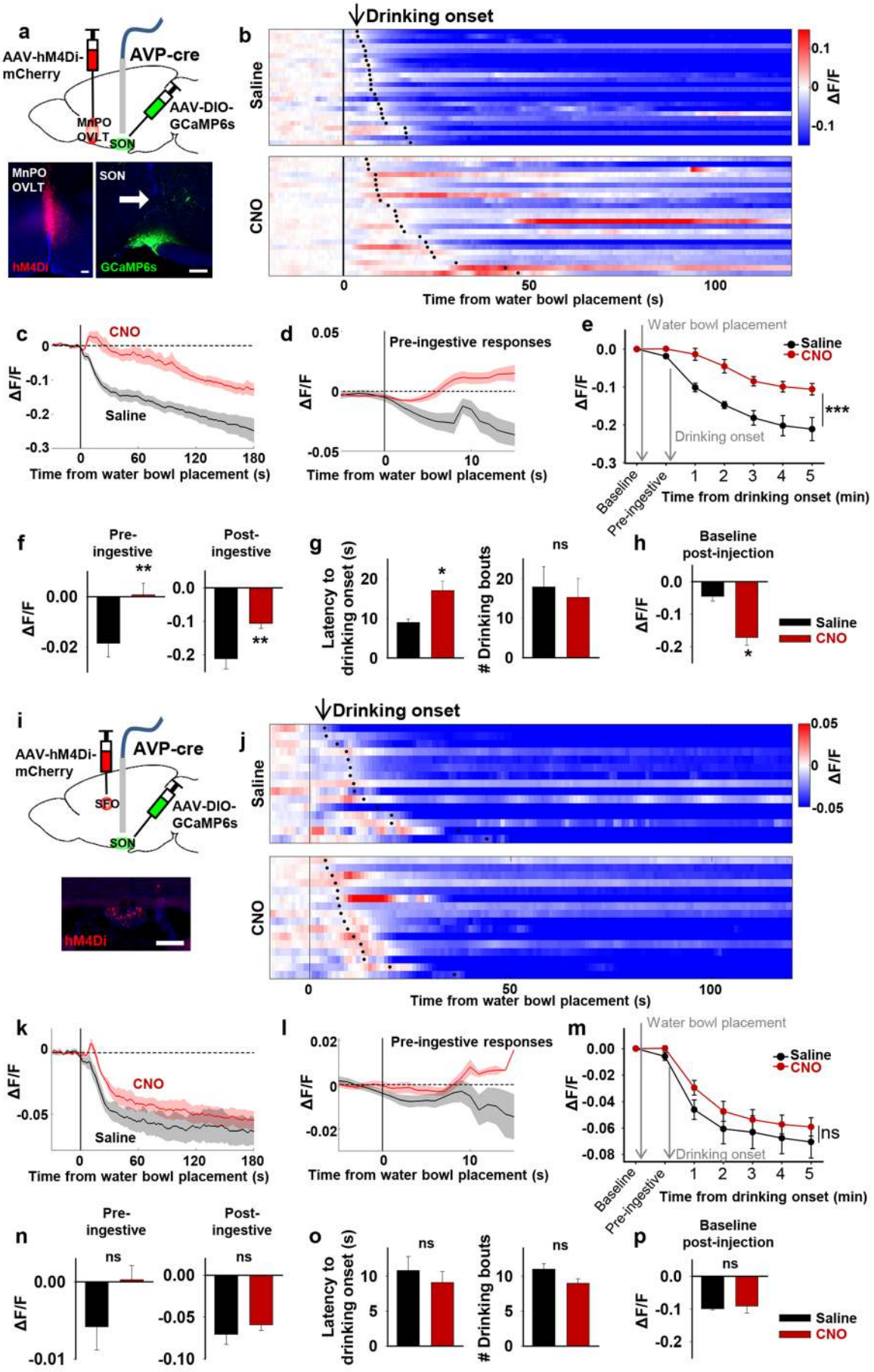

Figure 3

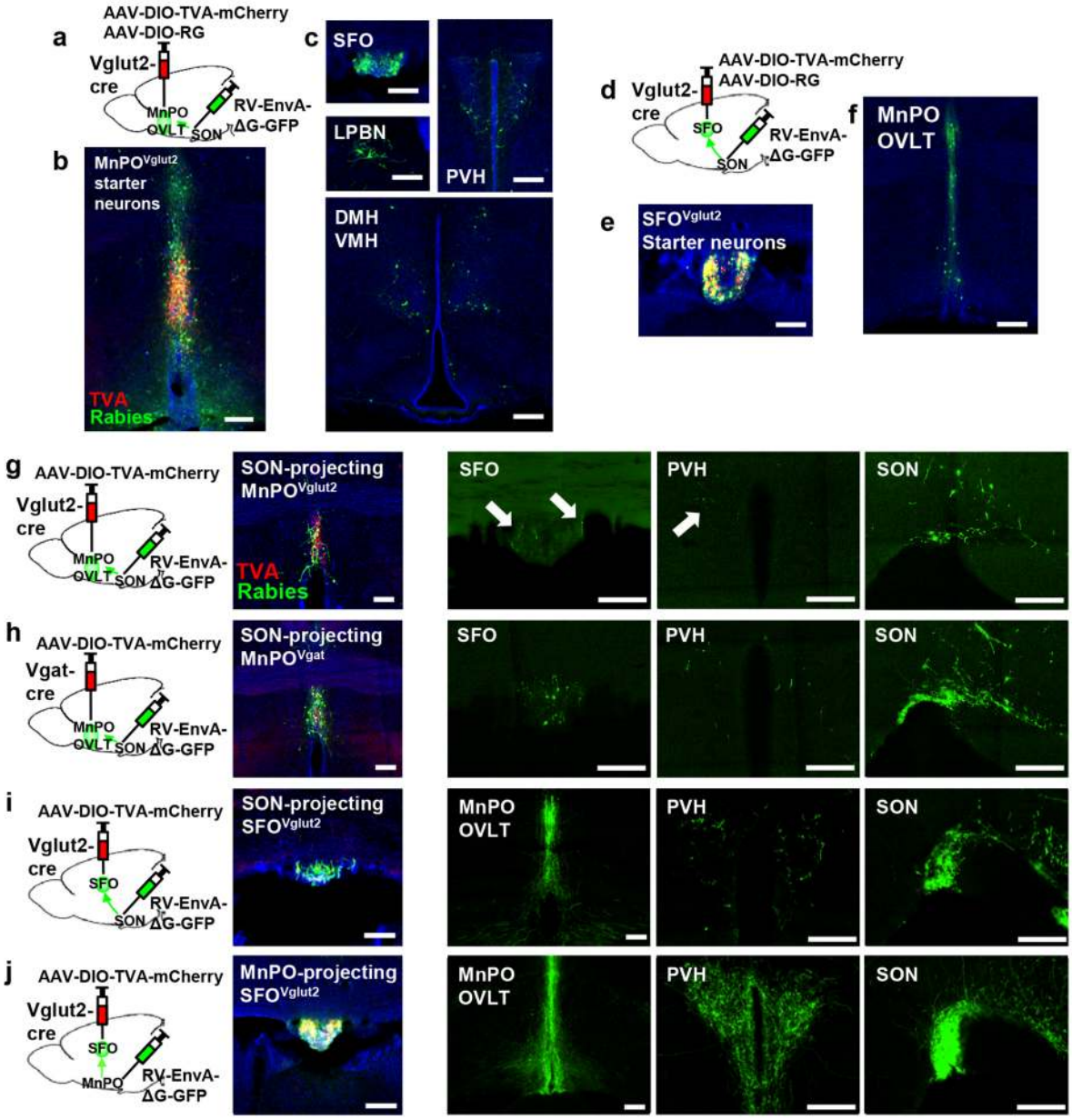

Figure 4

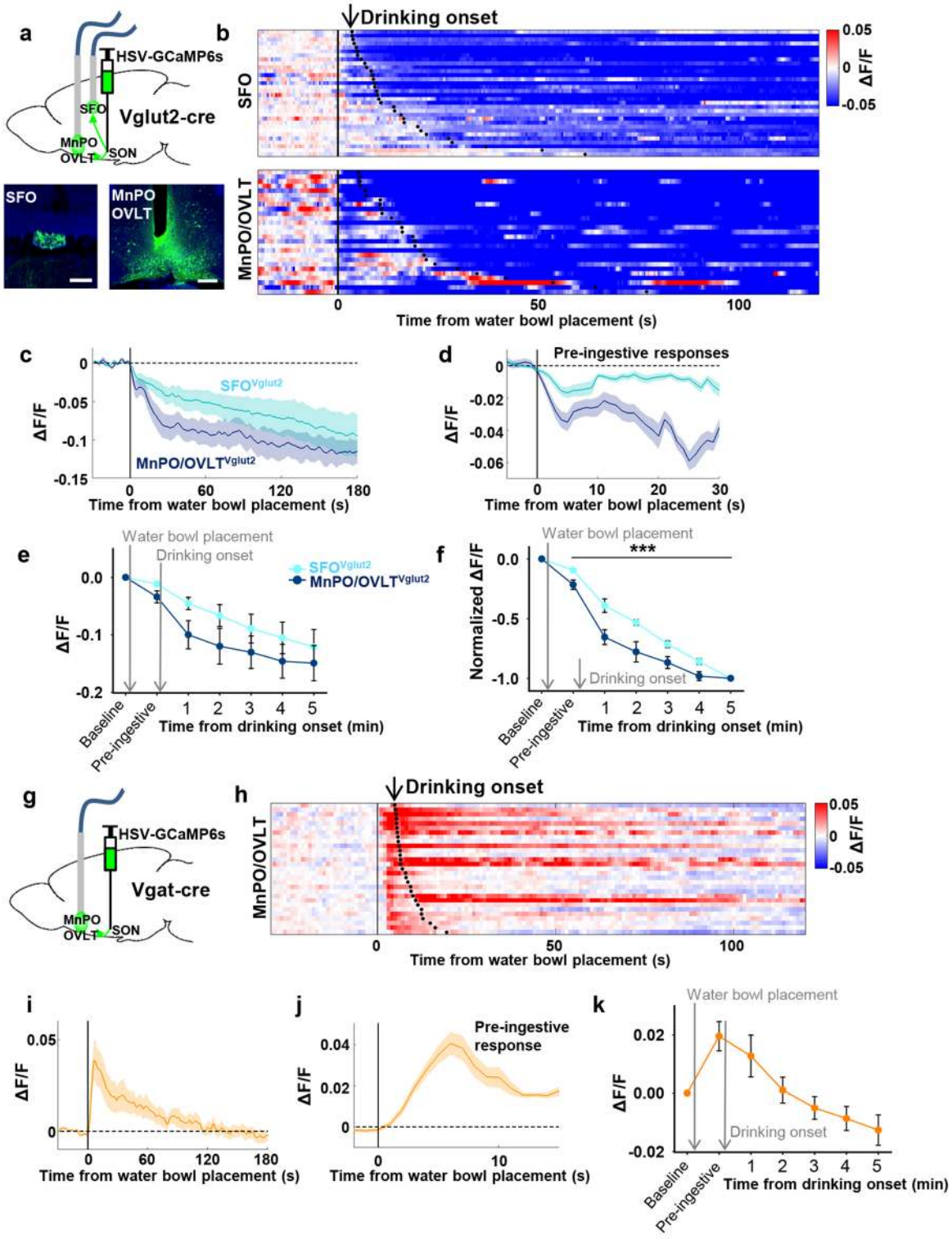

Figure 5

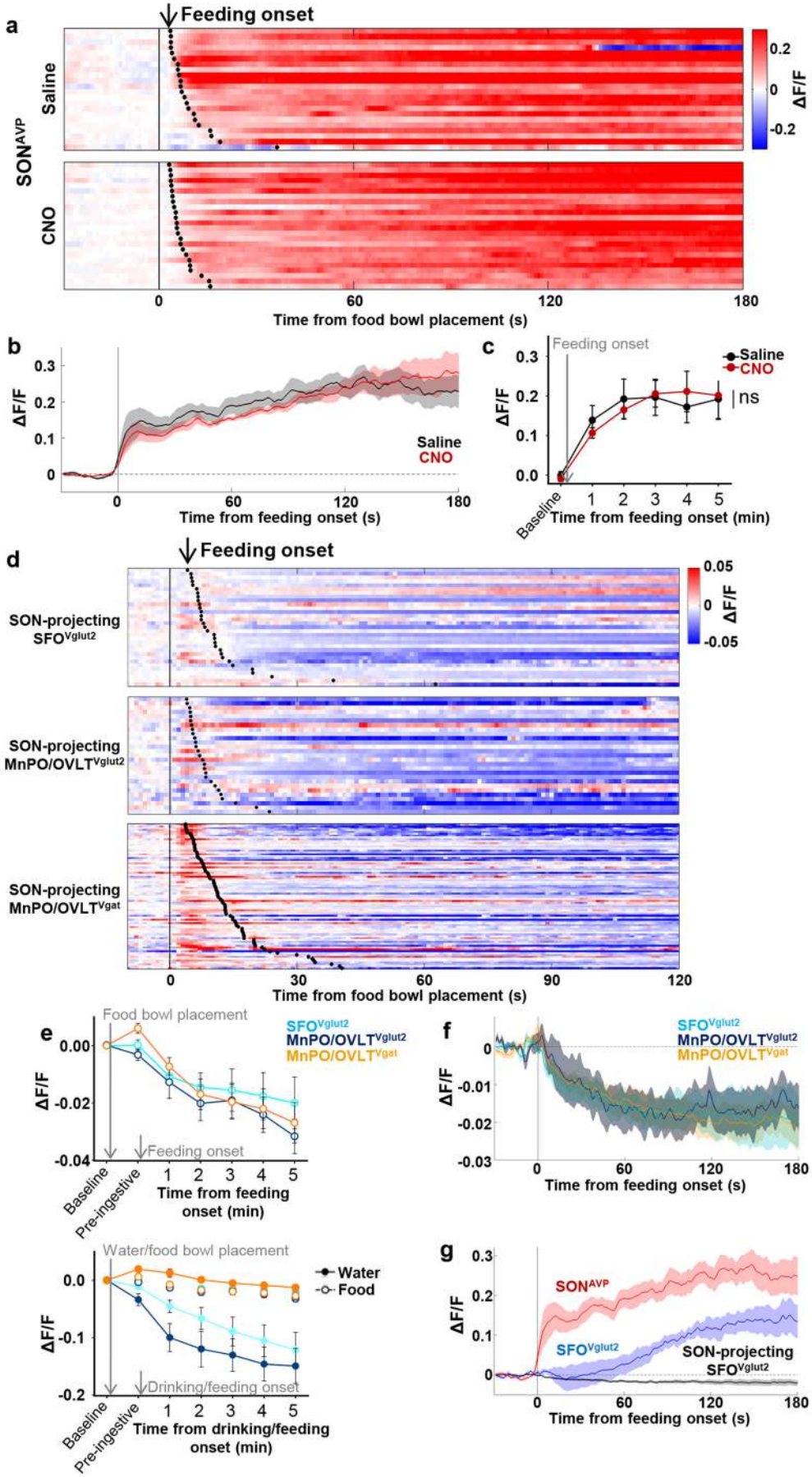

Figure 6

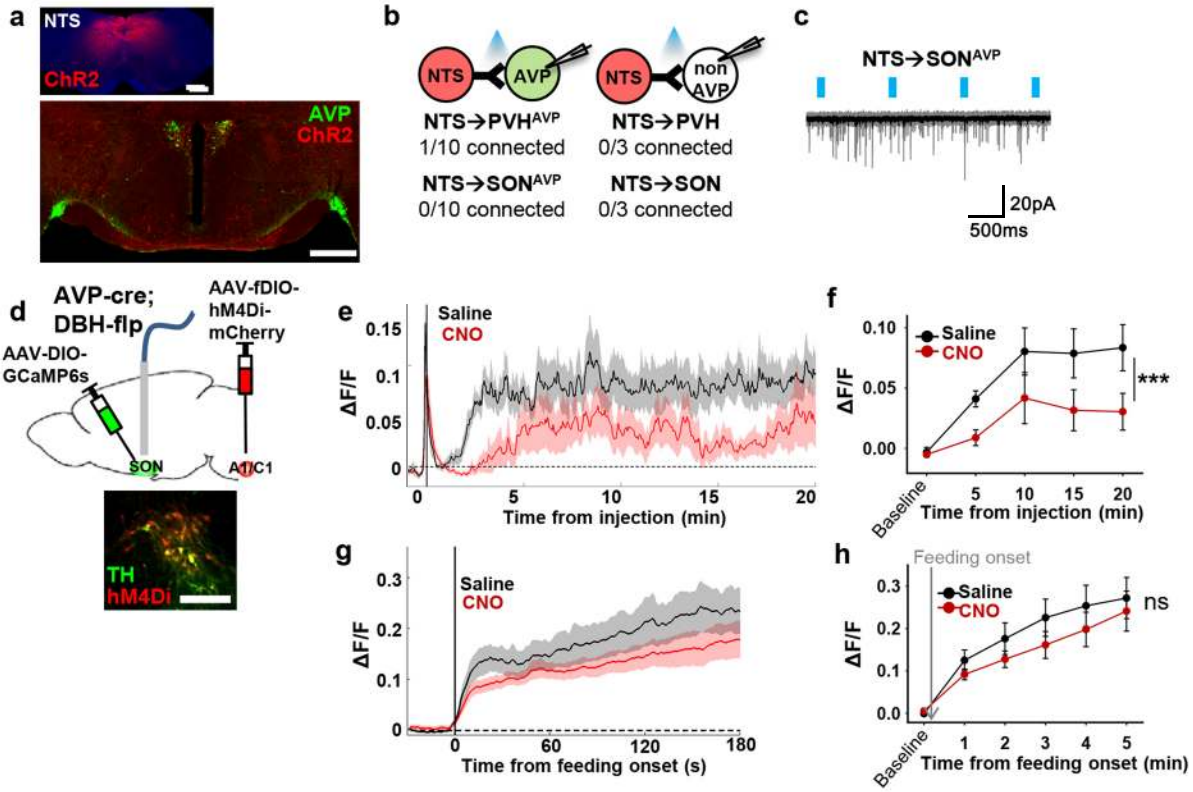

Figure 7

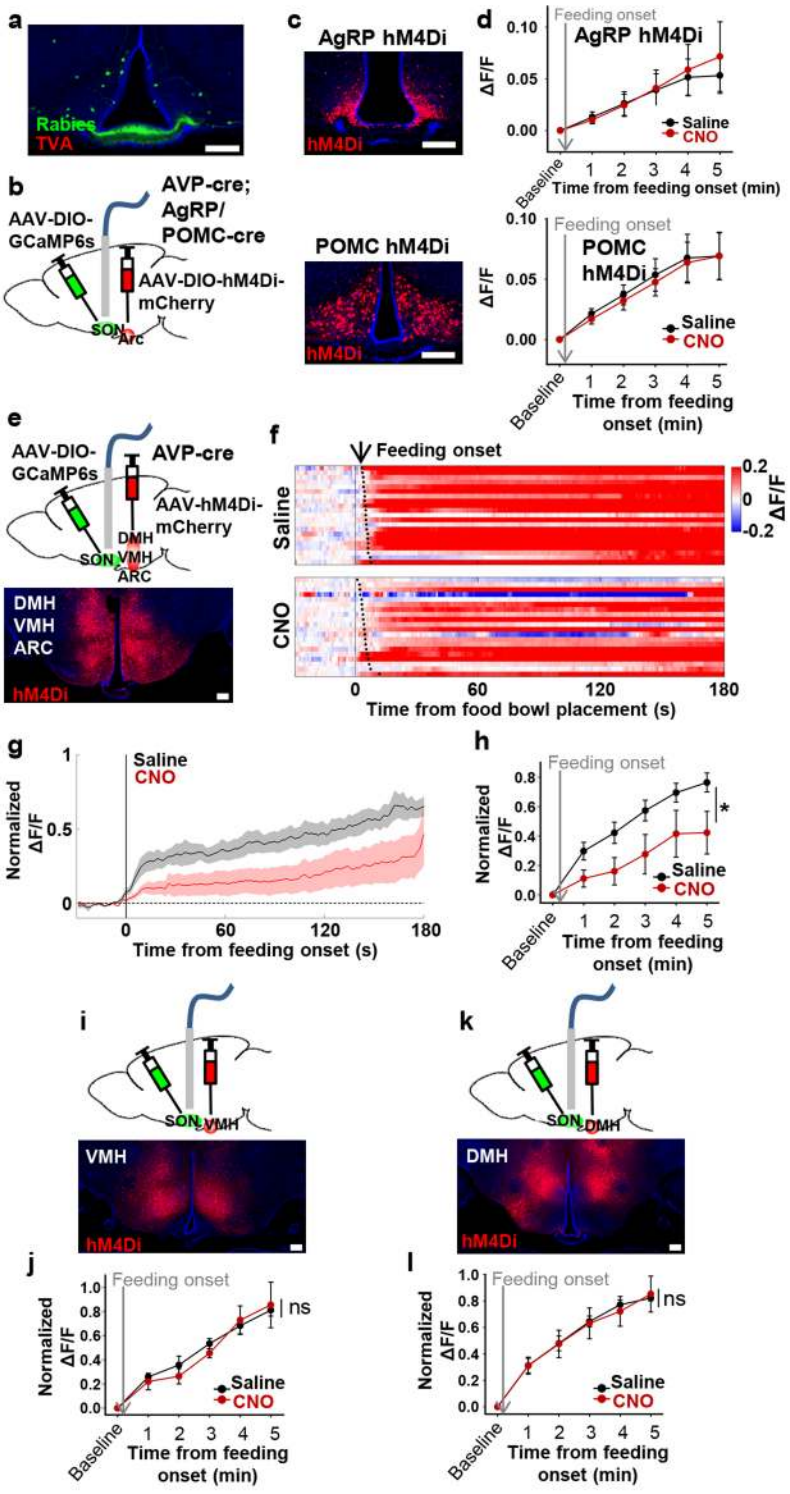

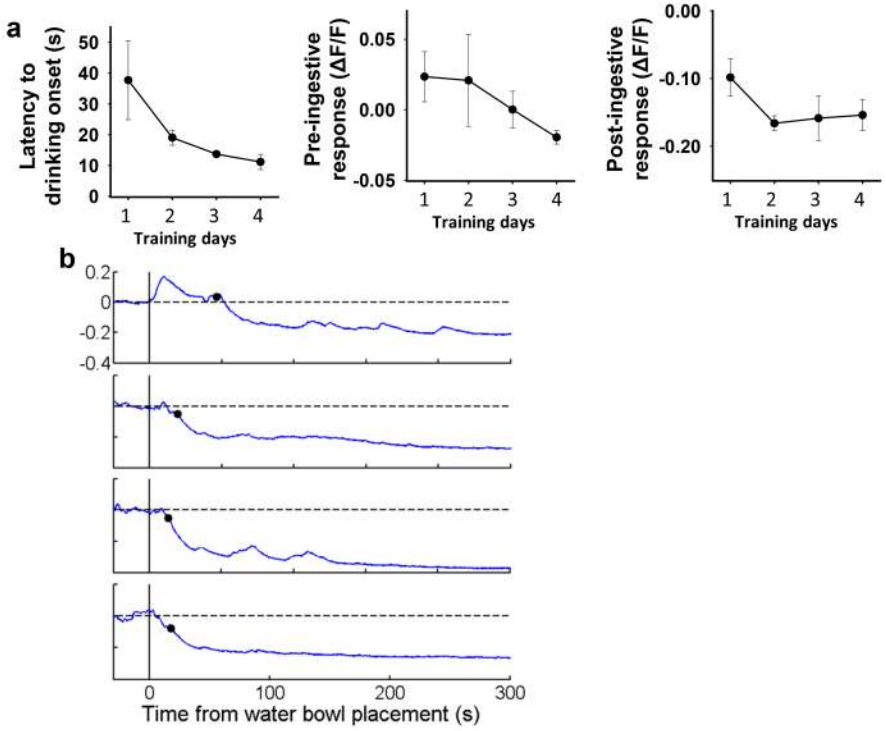

Figure 2—figure supplement 1 Pre-ingestive inhibition of SON^{AVP} neurons by water cue develops gradually over training.

a. Changes in latency to drinking onset, pre-ingestive and post-ingestive response of SON^{AVP} neurons over first 4 consecutive days of training.

b. Representative traces showing SON^{AVP} neuron activity in response to water bowl placement during first 4 consecutive days of training. Black circles indicate drinking onset. n= 4 mice.

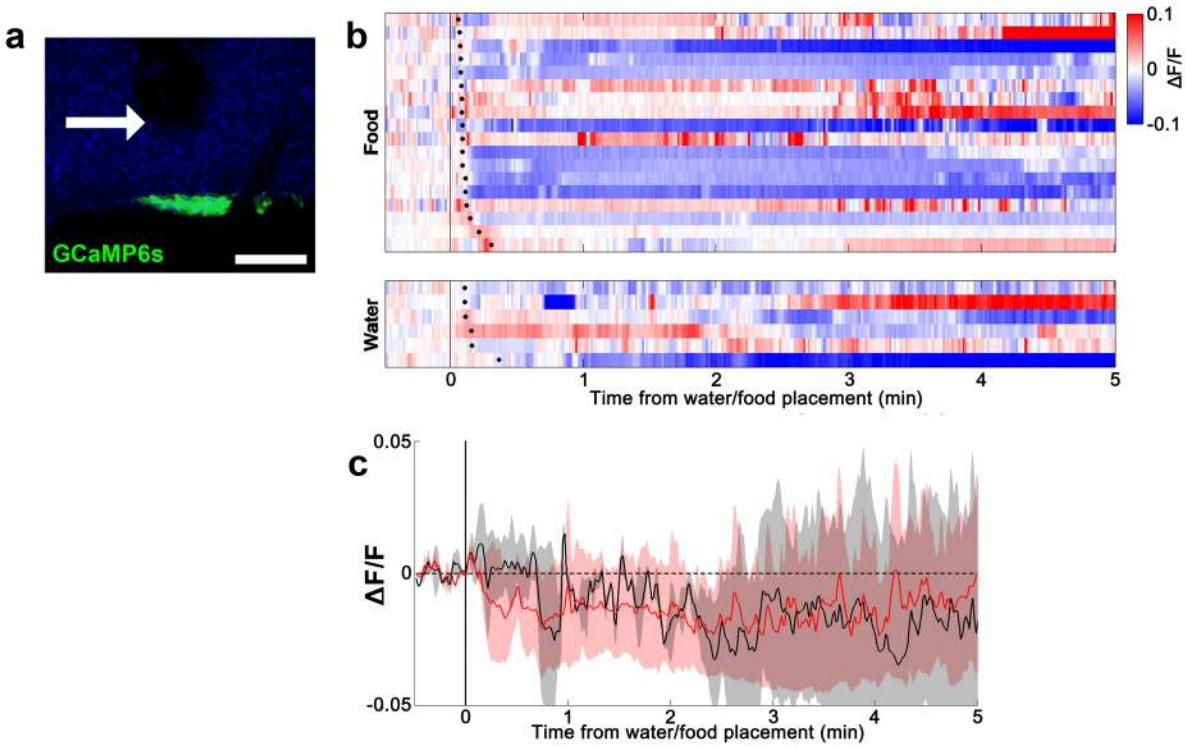

Figure 2—figure supplement 2 Lack of water- and food-induced responses in EYFP-expressing *AVP-IRES-Cre* mice.

a. Representative image showing EYFP expression in SON^{AVP} neurons.
b. Heatmap showing single-trial timecourses of fluorescence in response to water/food bowl placement. Trials are sorted according to latency from water/food bowl placement to drinking/feeding onset (black ticks).
c. Average fluorescence traces in response to water/food bowl placement.

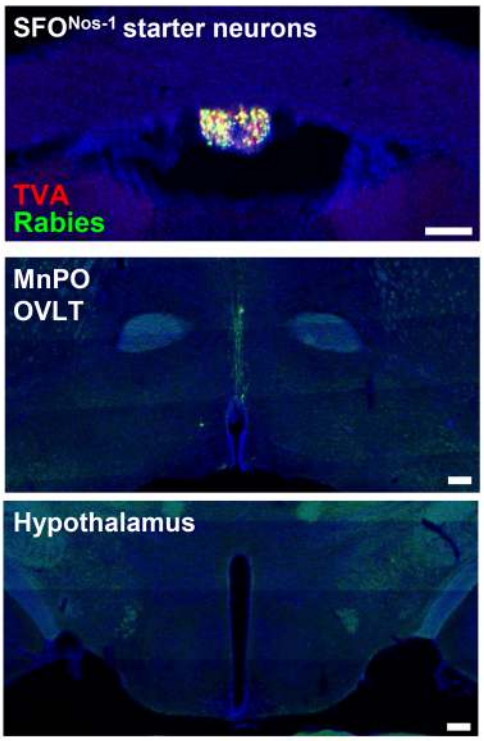

Figure 3—figure supplement 1 Monosynaptic rabies tracing from SON-projecting SFO^{Nos-1} neurons showing lack of extra LT afferents.

Representative image showing SFO^{Nos-1} starter neurons as identified by co-expression of GFP and mCherry (top), rabies-labeled neurons in the MnPO and OVLT that are monosynaptically connected to SFO^{Nos-1} neurons (middle), and lack of rabies-labeled neurons outside the LT as exemplified in the regions of hypothalamus (bottom). Scale bar, 200μm.

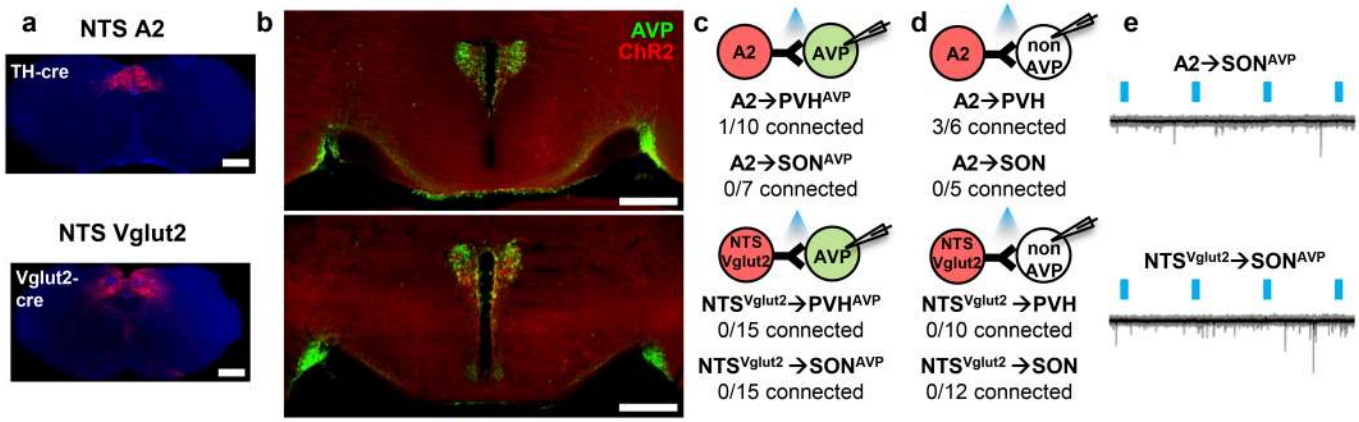

Figure 6—figure supplement 1 Monosynaptic rabies tracing from SON-projecting SFO^{Nos-1} neurons showing lack of extra LT afferents.

Representative image showing SFO^{Nos-1} starter neurons as identified by co-expression of GFP and mCherry (top), rabies-labeled neurons in the MnPO and OVLT that are monosynaptically connected to SFO^{Nos-1} neurons (middle), and lack of rabies-labeled neurons outside the LT as exemplified in the regions of hypothalamus (bottom). Scale bar, 200μm.

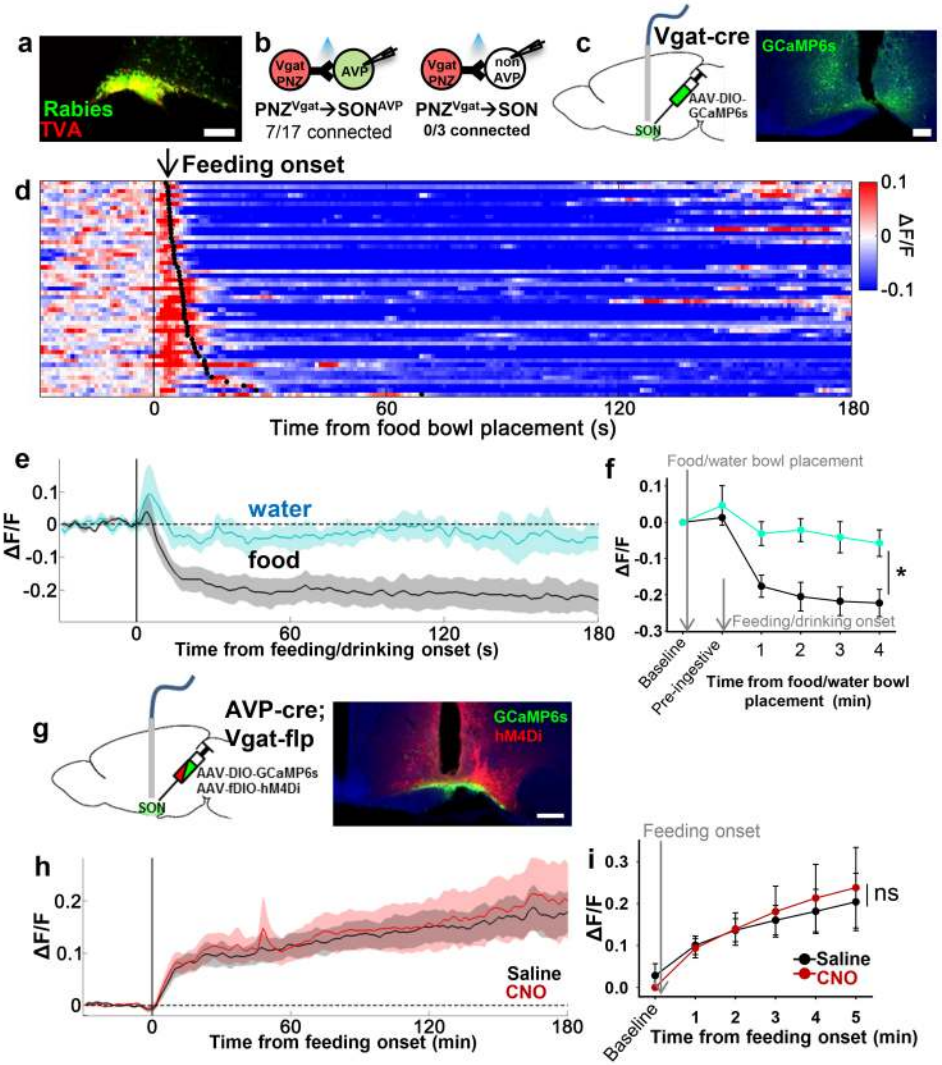

Figure 7—figure supplement 1 PNZ^{GABA} neurons show presystemic responses to feeding but are not required for food-related presystemic regulation of SON^{AVP} neurons.

a. Representative image showing rabies-labeled neurons in the PNZ that are monosynaptically connected to magnocellular SON^{AVP} neurons.
b. Number of SON^{AVP} neurons (left) and non-GFP SON neurons (right) receiving direct synaptic inputs from PNZ^{GABA} neurons as identified by CRACM in *AVP-GFP;Vgat-IRES-Cre*.
c. Schematic of PNZ^{GABA} photometry experiment.
d. Heatmap showing single-trial timecourses of PNZ^{GABA} population activity in response to food bowl placement. Trials are sorted according to latency from food bowl placement to feeding onset (black ticks). n= 8 mice.
e. Average PNZ^{GABA} population activity in response to water/food bowl placement. n= 3 mice.
f. Average PNZ^{GABA} population activity binned across drinking/feeding periods. *p < 0.05; 2-way ANOVA, n= 3 mice.

g. Schematic of SON^{AVP} photometry experiment with hM4Di-mediated inhibition of PNZ^{GABA} neurons.
h. Average of SON^{AVP} population activity in response to feeding onset in saline and CNO trials. n= 6 mice.
i. Average SON^{AVP} population activity binned across feeding periods in saline and CNO trials. ns, *p < 0.05; 2-way ANOVA, n= 6 mice.

Scale bar, 200μm. Values are means ± SEMs.

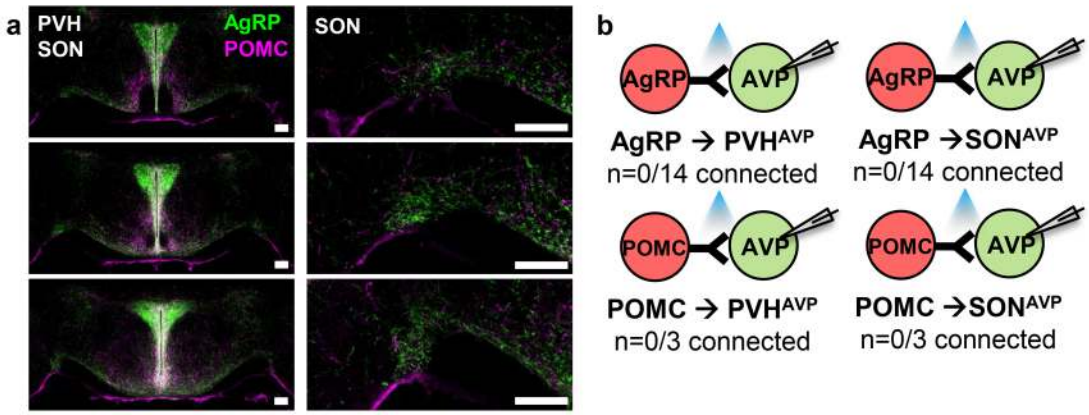

Figure 7—figure supplement 2 PVH^{AVP} and SON^{AVP} neurons do not receive direct synaptic inputs from AgRP and POMC neurons.

a. Projections of AgRP and POMC neurons in the PVH and SON identified by immunostaining (left). Magnified view of the SON showing presence of AgRP and POMC fibers (right).

b. Lack of direct synaptic connections between AgRP neurons and PVH^{AVP} and SON^{AVP} neurons as identified by CRACM in *AVP-GFP;Agrp-IRES-Cre*.

Scale bar, 200μm.

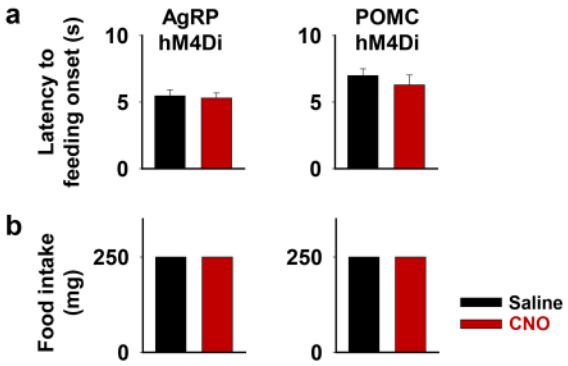

Figure 7—figure supplement 3 AgRP or POMC neuron inhibition does not affect short-term feeding behavior.

Latency to feeding onset (a) and amount of food intake during first 5 min of experiment (b) in saline and CNO trials of fiber photometry experiment with *AVP-IRES-Cre;AgRP/POMC-IRES-Cre* mice. One 250mg pellet was provided in all trials.